

Journal of Mechanics of Materials and Structures

**INSTABILITIES IN THE FREE INFLATION OF A
NONLINEAR HYPERELASTIC TOROIDAL MEMBRANE**

Sairam Pamulaparthi Venkata and Prashant Saxena

Volume 14, No. 4

July 2019



INSTABILITIES IN THE FREE INFLATION OF A NONLINEAR HYPERELASTIC TOROIDAL MEMBRANE

SAIRAM PAMULAPARTHI VENKATA AND PRASHANT SAXENA

We study an incompressible nonlinear hyperelastic thin-walled toroidal membrane of circular cross-section subjected to inflation due to a uniform pressure, comparing three elastic constitutive models (neo-Hookean, Mooney–Rivlin, and Ogden) and different torus shapes. A variational approach is used to derive the equations of equilibrium and bifurcation. An analysis of the pressure–deformation plots shows occurrence of the well-known limit point (snap-through) instabilities in the membrane. Calculations are performed to study the elastic buckling point to predict bifurcation of the solution corresponding to the loss of symmetry. Tension field theory is employed to study the wrinkling instability that, in this case, typically occurs near the inner regions of tori with large aspect ratios.

1. Introduction

Nonlinear elastic membranes are widely used to make engineering structures and occur naturally as biological tissues. Air bags, diaphragm valves, balloons, and soft tissues like skin, arterial walls, and cell walls are some examples. Large deformation due to inflation in membranes is typically associated with several instability modes and the behaviour strongly depends on the geometric and material nonlinearities. Here we study the inflation of an incompressible toroidal membrane under hydrostatic pressure and the instabilities accompanying large deformation. We present new results and analyses for different constitutive models, limit points, buckling, and wrinkling instabilities.

Axisymmetric deformations of toroidal membranes have been studied for several decades, for example, see the early works [Clark 1950; Jordan 1962; Liepins and Sanders 1963]. By using perturbation technique, an approximate solution for a thick-walled toroidal membrane made of neo-Hookean material is given in [Kydoniefs and Spencer 1965] and for a thin-walled toroidal membrane in [Kydoniefs and Spencer 1967]. Yang and Feng [1970] examined the problems concerning large axisymmetric deformations of nonlinear membranes of Mooney–Rivlin type by employing standard numerical techniques. Hill [1980] determined analytical solutions for a thick-walled toroidal membrane using the Mooney–Rivlin model. Asymptotic behaviour of a nonlinear torus was studied in [Bonadies 1987] using an assumption that overall radius of the torus is large in comparison to the radius of larger circle generating the torus. Application of finite-element formulation to numerically analyse axisymmetric incompressible nonlinear elastic membranes of general shape which exhibit finite strains can be found in the works [Wriggers and Taylor 1990; Gruttmann and Taylor 1992; Bařar and Itskov 1998]. Numerical studies by Holzapfel et al. [1996] and Humphrey [1998] shine light on remarkable success of the finite-element approach to understand axisymmetric nonlinear behaviour of anisotropic biomembranes and cells under

MSC2010: 74B20, 74G60, 74K15.

Keywords: membrane, limit point, wrinkling, bifurcation, nonlinear elasticity, finite deformation.

finite strain. Shang and Cheng [1991] employed Runge–Kutta numerical method followed by Newton–Raphson iterative technique to study axisymmetric deformation of hyperelastic toroidal membrane with finite strains by considering the volume of the gas inside the torus (monotonic function) as a control parameter instead of internal pressure (nonmonotonic function). Papargyri [1995] examined a pressurised compressible thin-walled nonlinear toroidal membrane by comparing the stability of analytical solution obtained from perturbation approach with the numerical results. Papargyri and Stavrakakis [2000] applied a numerical scheme to study an incompressible thin-walled nonlinear torus under internal pressure for different elastic constitutive models. Papargyri [2005] developed a finite-element method to numerically determine stresses and deformations in both compressible and incompressible thin-walled toroidal membrane under static inflation using Levenberg–Marquardt algorithm. By varying the geometric and material parameters, Tamadapu and DasGupta [2012] studied in-plane deformations in homogeneous inflated elastic toroidal membranes made of neo-Hookean and Mooney–Rivlin materials using discretisation methods for both isotropic and anisotropic cases. A direct integration method coupled with Nelder–Mead optimisation technique was formulated to determine numerical solutions for toroidal membranes in [Tamadapu and DasGupta 2014; Roychowdhury and DasGupta 2015].

Typical deformation characteristics of membranes under inflation involve the phenomenon of limit point or snap-through instability. A peak pressure is reached for a given deformation beyond which the membrane inflates rapidly with the slightest increase in pressure. These instabilities have been widely studied for membranes of various shapes [Benedict et al. 1979; Dreyer et al. 1982; Carroll 1987; Khayat et al. 1992; Müller and Struchtrup 2002]. Kanner and Horgan [2007] investigated the effect of strain-hardening on limit point instability in thin-walled spherical and cylindrical shells for different constitutive models and material parameters. Tamadapu et al. [2013] analysed the effects of geometric and material parameters on limit point pressure and the associated instabilities during inflation of incompressible nonlinear elastic membranes of Mooney–Rivlin type, including the torus. Reddy and Saxena [2017; 2018] employed both analytical and numerical schemes to study limit point instability in toroidal and cylindrical magnetoelastic membranes. Application of bifurcation theory to study buckling problems in the case of a general elastic deformation is a well-developed research area; see, for example, the classical works [Koiter 1945; Budiansky 1974].

During the process of stretching, a local structural instability in the form of wrinkling is typically observed in thin-walled elastic membranes for certain geometries and material parameters [Harold 1970; Szyszkowski and Glockner 1987; Jenkins et al. 1998]. Due to unequal stretching in the principal directions during inflation, compressive stresses may develop in certain regions of the membrane causing out of plane displacements. According to the tension field theory [Pipkin 1986], the wrinkles orient along the direction of the positive principal stress and the wrinkling occurs in the direction of negative principal stress. The component of principal stress along the direction of wrinkling is considered to be zero by Pipkin [1986]. Steigmann [1990] extended this theory to nonlinear elastic membranes and developed analytical functions to obtain information about stretch and the alignment of tension lines in membranes undergoing wrinkling. It is to be noted that, as no bending stiffness is assigned to the membrane, the amplitude and wavelength of the wrinkles cannot be computed by using this theory. Research on the wrinkling of membranes include [Stein and Hedgepeth 1961; Wu 1974; 1978; Wu and Canfield 1981; Mansfield 1981; Zak 1982; Haughton and McKay 1995; Epstein 1999; Saxena et al. 2019], to name a few. Axisymmetric deformations of tense and wrinkled zones in thin-walled

elastic isotropic membranes were found in Li and Steigmann [1995a; 1995b] using relaxed form of Ogden's three-terms strain energy model, by Roxburgh [1995] using relaxed form of Mooney–Rivlin strain energy function, and by Steigmann [2005] using relaxed form of Varga strain energy function. Wong and Pellegrino [2006] proposed an analytical method to determine the location of wrinkles and quantify the geometrical patterns such as amplitude and wavelength in linear elastic membranes. Nayyar et al. [2011] and Barsotti [2015] applied finite-element methods to study wrinkling in thin-walled elastic membranes. Patil et al. [2015] used a combination of standard and relaxed strain energy density functions to numerically determine the nonlinear axisymmetric deformations in tensed and wrinkled regions for an incompressible cylindrical membrane with nonuniform thickness. The numerical analysis was performed by applying finite difference method coupled with the Newton–Raphson iterative technique.

Here we analyse the influence of geometry and material parameters on axisymmetric deformations, limit points, bifurcation points, and wrinkling of inflated isotropic hyperelastic toroidal membrane under a uniform hydrostatic pressure. The two-point boundary value problem obtained from the equilibrium equations is converted to an initial value problem. Then, for a given deformation of a point on the outer equator of the membrane, the shooting method is employed to capture the unknown initial conditions using Nelder–Mead optimisation coupled with direct integration to solve the resulting equilibrium equations. We apply the classical theory of instability developed by Koiter [1945] and Budiansky [1974] by considering pressure as the loading parameter to compute the bifurcation point at which the symmetric fundamental solution becomes unstable. It is observed that bifurcation for torus of neo-Hookean type typically occurs very close to the limit point for the first mode except for the smallest aspect ratio case in which it occurs post limit point for the second mode. Location of wrinkled region is computed using an iterative process based on a kinematic condition that helps in an accurate recomputation of the entire solution using a coupled form of standard and relaxed energy to determine the membrane deformation.

Remainder of this paper is organised as follows. In Section 2, we formulate the problem statement along with the necessary kinematical equations for the reference and deformed configurations of the toroidal membrane. In Section 3, we formulate the governing equations of elastic equilibrium using the first variation of the total potential energy functional. We introduce three different elastic constitutive models (Ogden, Mooney–Rivlin, and neo-Hookean) used for computations and also derive the governing equations corresponding to wrinkling by using relaxed strain energy density. In Section 4, second variation of the strain-energy functional is derived for the neo-Hookean model to compute critical pressure for buckling. We discuss the numerical procedure used for computations and present our results and analysis in Section 5. Finally, we present the conclusions in Section 6.

2. Kinematics of deformation

Consider the reference and deformed configurations of an isotropic incompressible hyperelastic thin-walled toroidal membrane of a circular cross-section as shown in Figure 1. Smaller radius is R_s and the radius of revolution is R_b in the reference configuration. The toroidal membrane is inflated by an internal hydrostatic pressure. Thickness of the undeformed and deformed membranes are denoted by T and t , respectively related by the stretch ratio $\lambda_3 = t/T$. The thinness assumption requires $T \ll R_s$. Profile of the midsurface of torus in the deformed configuration can be traced using two functions \tilde{q} and $\tilde{\eta}$ as shown in the figure. The torus is symmetric about the Y^1 - Y^2 plane, hence we constrain the solution

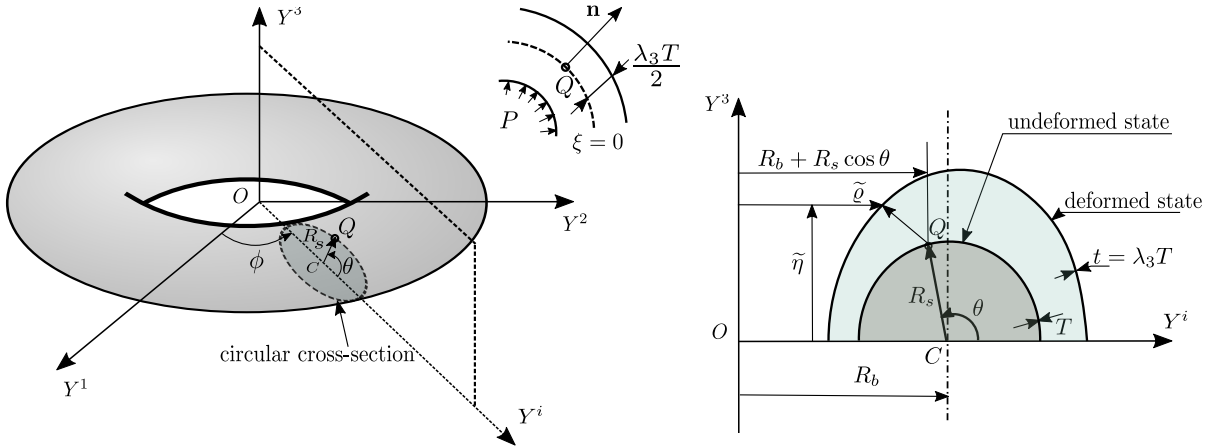


Figure 1. Toroidal membrane. Left: reference configuration, before deformation, with a circular cross-section highlighted. Right: slice of the membrane thickness acted upon by an internal pressure P . Top middle: Cross-section after general deformation illustrated through a point Q on Y^i - Y^3 plane. The membrane at any instant is symmetric about Y^1 - Y^2 plane and about the Y^3 axis.

space and study only the deformations of the toroidal membrane with respect to the upper half of the Y^1 - Y^2 plane. The calculations and notation below closely follow those in [Reddy and Saxena 2017].

It can be shown that the covariant metric tensors G_{ij} and \tilde{g}_{ij} in the reference and deformed configurations, respectively, are given by

$$[G_{ij}] = \begin{bmatrix} R_s^2 & 0 & 0 \\ 0 & R_b^2 R^2 & 0 \\ 0 & 0 & 1 \end{bmatrix}, \quad [\tilde{g}_{ij}] = \begin{bmatrix} \tilde{\varrho}_\theta^2 + \tilde{\eta}_\theta^2 & \tilde{\varrho}_\theta \tilde{\varrho}_\phi + \tilde{\eta}_\theta \tilde{\eta}_\phi & 0 \\ \tilde{\varrho}_\theta \tilde{\varrho}_\phi + \tilde{\eta}_\theta \tilde{\eta}_\phi & \tilde{\varrho}_\phi^2 + \tilde{\eta}_\phi^2 & 0 \\ 0 & 0 & \lambda_3^2 \end{bmatrix}, \quad (1)$$

where $R = [1 + R_s/R_b \cos \theta]$, and a subscript θ or ϕ denotes partial differentiation in that variable.

Upon introducing the nondimensional parameters

$$\gamma = R_s/R_b, \quad \varrho = \tilde{\varrho}/R_b, \quad \eta = \tilde{\eta}/R_b, \quad (2)$$

and applying the constraint of incompressibility $\det(\mathbf{F}) = 1$, \mathbf{F} being the deformation gradient tensor, we can write the principal stretch ratios $\lambda_1, \lambda_2, \lambda_3$ as

$$\begin{aligned} \lambda_1^2 &= \frac{1}{2} \left[\frac{\varrho_\theta^2 + \eta_\theta^2}{\gamma^2} + \frac{\varrho_\phi^2 + \eta_\phi^2 + \varrho^2}{R^2} \right] + \frac{1}{2} \sqrt{\left[\frac{\varrho_\theta^2 + \eta_\theta^2}{\gamma^2} - \frac{\varrho_\phi^2 + \eta_\phi^2 + \varrho^2}{R^2} \right]^2 + 4 \left[\frac{\varrho_\theta \varrho_\phi + \eta_\theta \eta_\phi}{\gamma R} \right]^2}, \\ \lambda_2^2 &= \frac{1}{2} \left[\frac{\varrho_\theta^2 + \eta_\theta^2}{\gamma^2} + \frac{\varrho_\phi^2 + \eta_\phi^2 + \varrho^2}{R^2} \right] - \frac{1}{2} \sqrt{\left[\frac{\varrho_\theta^2 + \eta_\theta^2}{\gamma^2} - \frac{\varrho_\phi^2 + \eta_\phi^2 + \varrho^2}{R^2} \right]^2 + 4 \left[\frac{\varrho_\theta \varrho_\phi + \eta_\theta \eta_\phi}{\gamma R} \right]^2}, \\ \lambda_3^2 &= \frac{1}{\lambda_1^2 \lambda_2^2} = \frac{\gamma^2 R^2}{\left[[\varrho_\theta^2 + \eta_\theta^2][\varrho_\phi^2 + \eta_\phi^2 + \varrho^2] - [\varrho_\theta \varrho_\phi + \eta_\theta \eta_\phi]^2 \right]} = \frac{\gamma^2 R^2}{[\varrho_\theta \eta_\phi - \varrho_\phi \eta_\theta]^2 + \varrho^2 [\varrho_\theta^2 + \eta_\theta^2]}. \end{aligned} \quad (3)$$

3. Energy considerations and governing equations

3.1. Potential energy and equilibrium equations. The total potential energy functional E of the system of interest is given by

$$E[\varrho, \eta] = T \int_{\Omega} W dA - \int_{V_0}^{V_0+\Delta V} \widehat{P} dV, \quad (4)$$

where T is the thickness of undeformed membrane, Ω represents the midsurface of the undeformed membrane, V_0 represents the enclosed initial volume and ΔV measures the change in the enclosed volume, $W(\varrho, \varrho_\theta, \varrho_\phi, \eta_\theta, \eta_\phi)$ is the strain energy per unit undeformed volume, and \widehat{P} is the hydrostatic pressure. Note that W has no explicit dependence on η since none of the principal stretch ratios depend on η as seen from (3).

Equation (4) can be rewritten as

$$E[\varrho, \eta] = T \int_0^{2\pi} \int_0^{2\pi} W \sqrt{G} d\theta d\phi - \int_0^{2\pi} \int_0^{2\pi} \widehat{P} \mathbf{n} da \cdot \delta \mathbf{y}, \quad (5)$$

where $\sqrt{G} = \sqrt{\det(G_{ij})} = RR_b$ and $da = \sqrt{g} d\theta d\phi$ is the area of a differential element on the deformed surface with the unit normal \mathbf{n} . Note that the strain energy is calculated over the reference configuration while the pressure work is evaluated over the deformed configuration.

First variation of the total potential energy is given as

$$\begin{aligned} \delta E = T \int_0^{2\pi} \int_0^{2\pi} & \left[\left[\frac{\partial W}{\partial \varrho} \sqrt{G} - \frac{\partial}{\partial \theta} \left(\frac{\partial W}{\partial \varrho_\theta} \sqrt{G} \right) - \frac{\partial}{\partial \phi} \left(\frac{\partial W}{\partial \varrho_\phi} \sqrt{G} \right) \right] \delta \varrho \right. \\ & \left. - \left[\frac{\partial}{\partial \theta} \left(\frac{\partial W}{\partial \eta_\theta} \sqrt{G} \right) + \frac{\partial}{\partial \phi} \left(\frac{\partial W}{\partial \eta_\phi} \sqrt{G} \right) \right] \delta \eta \right] d\theta d\phi \\ & + \int_0^{2\pi} \int_0^{2\pi} \widehat{P} R_b^3 [[\varrho_\theta] \delta \eta - [\eta_\theta] \delta \varrho] d\theta d\phi. \end{aligned} \quad (6)$$

From the principle of minimum potential energy, equilibrium states are attained when $\delta E = 0$ that results in the following Euler equations to be satisfied for evaluating the principal solution of deformation:

$$\frac{\partial}{\partial \theta} \left(\frac{\partial W}{\partial \varrho_\theta} \sqrt{G} \right) + \frac{\partial}{\partial \phi} \left(\frac{\partial W}{\partial \varrho_\phi} \sqrt{G} \right) - \frac{\partial W}{\partial \varrho} \sqrt{G} + \frac{\widehat{P} R_b^3}{T} [\varrho_\theta] = 0, \quad (7a)$$

$$\frac{\partial}{\partial \theta} \left(\frac{\partial W}{\partial \eta_\theta} \sqrt{G} \right) + \frac{\partial}{\partial \phi} \left(\frac{\partial W}{\partial \eta_\phi} \sqrt{G} \right) - \frac{\widehat{P} R_b^3}{T} [\varrho_\theta] = 0. \quad (7b)$$

The fundamental solution is symmetric with respect to rotation about the Y^3 axis resulting in $\varrho_\phi = \eta_\phi = 0$. Upon using this condition, (7a) is simplified to

$$\frac{\partial^2 W}{\partial \theta \partial \varrho_\theta} \gamma R - \frac{\partial W}{\partial \varrho_\theta} \gamma^2 \sin \theta - \frac{\partial W}{\partial \varrho} \gamma R + \frac{\widehat{P} R_b}{T} \varrho_\theta = 0, \quad (8)$$

and (7b) becomes

$$\frac{\partial^2 W}{\partial \theta \partial \eta_\theta} \gamma R - \frac{\partial W}{\partial \eta_\theta} \gamma^2 \sin \theta - \frac{\widehat{P} R_b}{T} \varrho_\theta = 0. \quad (9)$$

The governing equations (8) and (9) are solved using the boundary conditions which are determined based on compatibility and symmetry of the cross-section of the torus

$$\varrho_\theta(0) = \varrho_\theta(\pi) = 0, \quad \eta(0) = \eta(\pi) = 0. \tag{10}$$

3.1.1. Elastic constitutive models. In order to demonstrate mechanical behaviour via computations we use the three-term Ogden, Mooney–Rivlin, and neo-Hookean hyperelastic models for the elastic strain energy density W in this work. These are three very commonly used hyperelastic energy density functions in several computational studies [Holzapfel 2000]. The mathematical expressions and numerical values of the material parameters are given below.

The strain energy density for the three-term Ogden model is given by

$$W^*(\lambda_1, \lambda_2) = \sum_{j=1}^3 \frac{\mu_j}{\alpha_j} \left[\lambda_1^{\alpha_j} + \lambda_2^{\alpha_j} + \left[\frac{1}{\lambda_1 \lambda_2} \right]^{\alpha_j} - 3 \right], \tag{11}$$

along with the conditions $\sum_j \mu_j \alpha_j = 2\mu$ and $\mu_j \alpha_j > 0$. The nondimensional parameters can be defined as $\mu_1^* = \mu_1/\mu$, $\mu_2^* = \mu_2/\mu$, $\mu_3^* = \mu_3/\mu$, where μ is the baseline shear modulus.

Upon substituting $\alpha_1 = 2$, $\alpha_2 = -2$, and $\mu_3 = 0$ in (11), we arrive at the Mooney–Rivlin strain energy density given by

$$W^*(\lambda_1, \lambda_2) = \frac{1}{2}\mu_1 \left[\lambda_1^2 + \lambda_2^2 + \frac{1}{\lambda_1^2 \lambda_2^2} - 3 \right] - \frac{1}{2}\mu_2 \left[\frac{1}{\lambda_1^2} + \frac{1}{\lambda_2^2} + \lambda_1^2 \lambda_2^2 - 3 \right]. \tag{12}$$

Upon using $\alpha_1 = 2$, $\mu_2 = \mu_3 = 0$ in (11), we arrive at the neo-Hookean strain energy density given by

$$W^*(\lambda_1, \lambda_2) = \frac{1}{2}\mu_1 \left[\lambda_1^2 + \lambda_2^2 + \frac{1}{\lambda_1^2 \lambda_2^2} - 3 \right]. \tag{13}$$

Upon substitution of the explicit expressions of each of the above energy density functions, the resulting governing equations (8) and (9) can be rewritten as a system of first-order ODEs in matrix form as

$$\begin{bmatrix} 1 & 0 & 0 & 0 \\ 0 & S_{22} & 0 & S_{24} \\ 0 & 0 & 1 & 0 \\ 0 & S_{42} & 0 & S_{44} \end{bmatrix} \begin{bmatrix} \mathcal{U}'_1 \\ \mathcal{U}'_2 \\ \mathcal{U}'_3 \\ \mathcal{U}'_4 \end{bmatrix} = \begin{bmatrix} \mathcal{U}_2 \\ \mathcal{V}_1 \\ \mathcal{U}_4 \\ \mathcal{V}_2 \end{bmatrix}, \tag{14}$$

where

$$\mathcal{U}_1 = \varrho, \quad \mathcal{U}_2 = \varrho_\theta = \mathcal{U}'_1, \quad \mathcal{U}'_2 = \varrho_{\theta\theta}, \quad \mathcal{U}_3 = \eta, \quad \mathcal{U}_4 = \eta_\theta = \mathcal{U}'_3, \quad \mathcal{U}'_4 = \eta_{\theta\theta}, \tag{15}$$

and the remaining terms S_{22} , S_{24} , S_{42} , S_{44} , \mathcal{V}_1 , \mathcal{V}_2 for each of the constitutive models are listed in Sections A.1–A.3 in the Appendix.

3.2. Relaxed strain energy density. During the inflation of elastic membranes, compressive stresses might develop for certain geometries as the membrane undergoes unequal stretching in the principal directions. As membranes are no-compression structures, these in-plane negative stresses result in out of plane deformations causing wrinkling instability. According to the tension field theory, with the absence of bending stiffness in thin membranes, infinitesimally small and closely spaced wrinkles are formed due to compressive stresses. We observe the compressive stresses for certain geometries and for specific

material parameters in our study. Pipkin [1986] proposed the concept of “relaxed strain energy density” by modifying the elastic constitutive relation based on principal stretches to study the wrinkling behaviour in linear elastic membranes. This theory is extended to nonlinear elastic membranes by Steigmann [1990]. The relaxed strain energy density W_R is represented as

$$W_R = \begin{cases} W(\lambda_1, \lambda_2) & \text{if } \lambda_2 \geq w(\lambda_1) \text{ and } \lambda_1 \geq w(\lambda_2), \\ W_t(\lambda_1) & \text{if } \lambda_2 \leq w(\lambda_1) \text{ and } \lambda_1 \geq 1, \\ W_t(\lambda_2) & \text{if } \lambda_1 \leq w(\lambda_2) \text{ and } \lambda_2 \geq 1, \\ 0 & \text{if } \lambda_1 \leq 1 \text{ and } \lambda_2 \leq 1, \end{cases} \tag{16}$$

where the function $w(\lambda)$ is termed as the “natural width in simple tension” and defined below. For any fixed value of λ_1 , the minimum of W with respect to λ_2 is attained at

$$\lambda_2 = \lambda_1^{-1/2} =: w(\lambda_1). \tag{17}$$

Similarly, for any fixed value of λ_2 , the minimum of W with respect to λ_1 is attained at

$$\lambda_1 = \lambda_2^{-1/2} = w(\lambda_2). \tag{18}$$

As compressive stresses develop in the region $\lambda_1 \geq 1$ and $\lambda_2 \leq w(\lambda_1)$, we can replace the original strain energy density function W by $W_t(\lambda_1)$ as mentioned in (16).

The terms $S_{22}, S_{24}, S_{42}, S_{44}, \nu_1, \nu_2$ in the governing equation (14) for computations in the wrinkled region should be modified according to the above-stated conditions and are given in Appendix A.4.

4. Second variation of total potential energy functional

In elastic solids, we often observe critical (buckling) points for certain load values at which the equilibrium path branches out into multiple stable and/or unstable paths. These critical points are of considerable interest as the postbuckling response of the system is usually different from the initial response (principal solution). Considering the hydrostatic pressure as a loading parameter, we adopt the procedure proposed in [Budiansky 1974] to determine the critical pressure in our case of hyperelastic membrane beyond which the symmetric fundamental solution is no longer the energy minimiser. To reduce the complexity of long mathematical expressions, we study the critical pressure condition only for the neo-Hookean material model.

4.1. Critical pressure. The fundamental solution for ϱ and η is symmetric with respect to the Y^3 axis and therefore has no dependence on ϕ . We define critical pressure as the point where the solution loses this symmetry while retaining the symmetry with respect to the Y^1 - Y^2 plane. Hence, we consider the bifurcation branches that include perturbations in the ϕ direction. The following expansions are considered for the variables ϱ and η :

$$\begin{aligned} \varrho(\theta, \phi) &= \varrho_0(\theta) + \hat{\varrho}(\phi) = \varrho_0(\theta) + \Upsilon \varrho_1(\phi) + \dots \\ \eta(\theta, \phi) &= \eta_0(\theta) + \hat{\eta}(\phi) = \eta_0(\theta) + \Upsilon \eta_1(\phi) + \dots \\ \Upsilon &= \langle \hat{\varrho}, \varrho_1 \rangle = \langle \hat{\eta}, \eta_1 \rangle, \quad \langle \varrho_i, \varrho_j \rangle = \langle \eta_i, \eta_j \rangle = \begin{cases} 1 & \text{if } i = j, \\ 0 & \text{otherwise,} \end{cases} \end{aligned} \tag{19}$$

where the scalar parameter $\Upsilon \ll 1$ measures the amount of bifurcation mode, $\langle \bullet \rangle$ represents a suitable inner product, and ϱ_1 and η_1 represent the first bifurcation mode with ϱ_0 and η_0 being the fundamental states.

Bifurcation of the solution occurs when the second variation of the potential energy vanishes. For the current scenario, it is given as

$$\delta^2 E = E''_{c'} U_1 \delta U = [E''_{c_{\alpha_1}} + E''_{c_{\alpha_2}} - E''_{c_{\alpha_31}} - E''_{c_{\alpha_32}} + E''_{c_{\alpha_33}} + E''_{c_{\alpha_34}}] U_1 \delta U + [-E''_{c_{\alpha_35}} + E''_{c_{\alpha_36}} + E''_{c_p}] U_1 \delta U = 0, \quad (20)$$

where we have defined several terms as below

$$E''_{c_{\alpha_1}} U_1 \delta U = 0, \quad (21)$$

$$E''_{c_{\alpha_2}} U_1 \delta U = 2\bar{\mu}T \int_0^{2\pi} \int_0^{2\pi} \frac{\varrho_{1\phi} \delta \varrho_\phi + \eta_{1\phi} \delta \eta_\phi + \varrho_1 \delta \varrho}{R^2} \sqrt{G} d\theta d\phi, \quad (22)$$

$$E''_{c_{\alpha_31}} U_1 \delta U = 2\bar{\mu}T \gamma^2 \int_0^{2\pi} \int_0^{2\pi} \frac{\mathcal{E}_{aa} \mathcal{E}_{ab}}{\mathcal{E}_{ac}^2} \sqrt{G} R^2 d\theta d\phi, \quad (23)$$

$$E''_{c_{\alpha_32}} U_1 \delta U = 2\bar{\mu}T \gamma^2 \int_0^{2\pi} \int_0^{2\pi} \frac{[\varrho_\theta \eta_\phi - \varrho_\phi \eta_\theta][\eta_{1\phi} \delta \varrho_\theta - \varrho_{1\phi} \delta \eta_\theta]}{\mathcal{E}_{ac}^2} \sqrt{G} R^2 d\theta d\phi, \quad (24)$$

$$E''_{c_{\alpha_33}} U_1 \delta U = 8\bar{\mu}T \gamma^2 \int_0^{2\pi} \int_0^{2\pi} \frac{[\varrho_\theta \eta_\phi - \varrho_\phi \eta_\theta]^2 \mathcal{E}_{aa} \mathcal{E}_{ab}}{\mathcal{E}_{ac}^3} \sqrt{G} R^2 d\theta d\phi, \quad (25)$$

$$E''_{c_{\alpha_34}} U_1 \delta U = 8\bar{\mu}T \gamma^2 \int_0^{2\pi} \int_0^{2\pi} \frac{[\varrho_\theta \eta_\phi - \varrho_\phi \eta_\theta] \mathcal{E}_{ad} \mathcal{E}_{ab}}{\mathcal{E}_{ac}^3} \sqrt{G} R^2 d\theta d\phi, \quad (26)$$

$$E''_{c_{\alpha_35}} U_1 \delta U = 2\bar{\mu}T \gamma^2 \int_0^{2\pi} \int_0^{2\pi} \frac{\varrho_1 [\varrho_\theta^2 + \eta_\theta^2] \delta \varrho + 2\varrho \varrho_1 [\varrho_\theta \delta \varrho_\theta + \eta_\theta \delta \eta_\theta]}{\mathcal{E}_{ac}^2} \sqrt{G} R^2 d\theta d\phi, \quad (27)$$

$$E''_{c_{\alpha_36}} U_1 \delta U = 8\bar{\mu}T \gamma^2 \int_0^{2\pi} \int_0^{2\pi} \frac{\varrho \varrho_1 [\varrho_\theta^2 + \eta_\theta^2][[\varrho_\theta \eta_\phi - \varrho_\phi \eta_\theta] \mathcal{E}_{aa} + \mathcal{E}_{ad}]}{\mathcal{E}_{ac}^3} \sqrt{G} R^2 d\theta d\phi, \quad (28)$$

$$E''_{c_p} U_1 \delta U = \int_0^{2\pi} \int_0^{2\pi} \hat{P} R_b^3 [\varrho_\theta \eta_1 \delta \varrho + \varrho \eta_1 \delta \varrho_\theta - \eta_\theta \varrho_1 \delta \varrho - \varrho \varrho_1 \delta \eta_\theta] d\theta d\phi, \quad (29)$$

with

$$\begin{aligned} \mathcal{E}_{aa} &= \eta_\phi \delta \varrho_\theta + \varrho_\theta \delta \eta_\phi - \eta_\theta \delta \varrho_\phi - \varrho_\phi \delta \eta_\theta, & \mathcal{E}_{ab} &= \varrho_\theta \eta_{1\phi} - \eta_\theta \varrho_{1\phi}, & \bar{\mu} &= \frac{1}{2} \mu_1, \\ \mathcal{E}_{ac} &= [\varrho_\theta \eta_\phi - \varrho_\phi \eta_\theta]^2 + \varrho^2 [\varrho_\theta^2 + \eta_\theta^2], & \mathcal{E}_{ad} &= \varrho [\varrho_\theta^2 + \eta_\theta^2] \delta \varrho + \varrho^2 [\varrho_\theta \delta \varrho_\theta + \eta_\theta \delta \eta_\theta]. \end{aligned} \quad (30)$$

Upon separating the coefficients of $\delta \varrho$ and $\delta \eta$, we obtain the following governing equations for the bifurcated mode

$$\mathcal{K}_{aa} \varrho_1 + \mathcal{K}_{bb} \varrho_{1\phi\phi} + \mathcal{K}_{cc} \eta_{1\phi\phi} = 0, \quad (31)$$

and

$$\mathcal{L}_{aa} \varrho_1 + \mathcal{L}_{bb} \varrho_{1\phi\phi} + \mathcal{L}_{cc} \eta_{1\phi\phi} = 0, \quad (32)$$

| |
|---|
| Three-term Ogden model [1972]: $\begin{aligned} \mu_1^* &= 1.4910, & \mu_2^* &= 0.0029, & \mu_3^* &= -0.0236, \\ \alpha_1 &= 1.3, & \alpha_2 &= 5.0, & \alpha_3 &= -2.0, \end{aligned}$ |
| Mooney–Rivlin model: $\mathfrak{M} = -\frac{\mu_2}{\mu_1} = 0.1$ and 0.3 . |

Table 1. Nondimensional material parameters used for numerical computations.

where the bifurcation pressure is denoted as \widehat{P}_c and

$$\begin{aligned} \mathcal{K}_{aa} &= R\gamma\varrho^4\mathcal{N}^3 + 3R^5\gamma^3\mathcal{N}^2 + 6\varrho_\theta^2R^5\gamma^3\mathcal{N} - 2\varrho\varrho_{\theta\theta}R^5\gamma^3\mathcal{N} + 6\varrho\varrho_\theta R^4\gamma^4\mathcal{N} \sin\theta \\ &\quad + 8\varrho\varrho_\theta[\varrho_\theta\varrho_{\theta\theta} + \eta_\theta\eta_{\theta\theta}]R^5\gamma^3 - \frac{1}{2}P_c\eta_\theta R^2\varrho^4\mathcal{N}^3, \\ \mathcal{K}_{bb} &= -\varrho^4\gamma R\mathcal{N}^3 + \eta_\theta^2R^5\gamma^3\mathcal{N}, & \mathcal{K}_{cc} &= -\varrho_\theta\eta_\theta R^5\gamma^3\mathcal{N}, \\ \mathcal{N} &= \varrho_\theta^2 + \eta_\theta^2, & P_c &= \frac{\widehat{P}_c R_b}{\bar{\mu}T}, \\ \mathcal{L}_{aa} &= 6\varrho_\theta\eta_\theta R^5\gamma^3\mathcal{N} - 2\varrho\eta_{\theta\theta}R^5\gamma^3\mathcal{N} + 6\varrho\eta_\theta R^4\gamma^4\mathcal{N} \sin\theta + 8\varrho\eta_\theta[\varrho_\theta\varrho_{\theta\theta} + \eta_\theta\eta_{\theta\theta}]R^5\gamma^3 + \frac{1}{2}P_c\varrho^4\varrho_\theta R^2\mathcal{N}^3, \\ \mathcal{L}_{bb} &= -\varrho_\theta\eta_\theta R^5\mathcal{N}^3, & \mathcal{L}_{cc} &= -\gamma R\varrho^4\mathcal{N}^3 + \varrho_\theta^2R^5\gamma^3\mathcal{N}. \end{aligned} \tag{33}$$

Upon considering the following ansatz for ϱ_1 and η_1 :

$$\varrho_1 = \varrho_1^0 \exp(in\phi), \quad \eta_1 = \eta_1^0 \exp(in\phi), \quad \text{where } i = \sqrt{-1}. \tag{34}$$

It can be shown that a nontrivial solution for the above system of equation exists when

$$\mathcal{R}_{\text{res}} = [[\mathcal{K}_{cc}\mathcal{L}_{aa} - \mathcal{K}_{aa}\mathcal{L}_{cc}] + n^2[\mathcal{K}_{bb}\mathcal{L}_{cc} - \mathcal{K}_{cc}\mathcal{L}_{bb}]] = 0. \tag{35}$$

The residue \mathcal{R}_{res} defined above should be put to zero computationally in order to calculate the critical pressure value.

5. Numerical procedure, results, and discussion

Computations are performed for numerical values of the material parameters presented in Table 1.

5.1. Calculation of fundamental solution. The governing equations (8) and (9) for fundamental solution are subjected to boundary conditions defined by (10). They are numerically solved for three elastic constitutive models (Ogden, Mooney–Rivlin, and neo-Hookean) by following a method used for similar problems in [Tamadapu and DasGupta 2014; Reddy and Saxena 2017]. The two point boundary value problem is converted into an initial value problem with two unknown parameters $(\varrho(0), \eta_\theta(0))$ at a particular nondimensional pressure P . For a given value of location of point on the outer equator of the membrane $(\varrho(0) > 1 + \gamma)$, we start with an initial guess for the pair $(\eta_\theta(0), P)$, and employ shooting method to obtain the two boundary values $\varrho_\theta(\pi)$ and $\eta(\pi)$ for the point on the inner edge. Ideally $\varrho_\theta(\pi)$ and $\eta(\pi)$ should be zero. The desired optimisation pair $(\eta_\theta(0), P)$ which reduces the value of the cost function, $[\varrho_\theta(\pi)^2 + \eta(\pi)^2]^{1/2}$, to a sufficiently small quantity ($< \mathcal{O}(10^{-12})$) is obtained by using the Nelder–Mead simplex optimisation technique of two variables. This optimisation method is performed

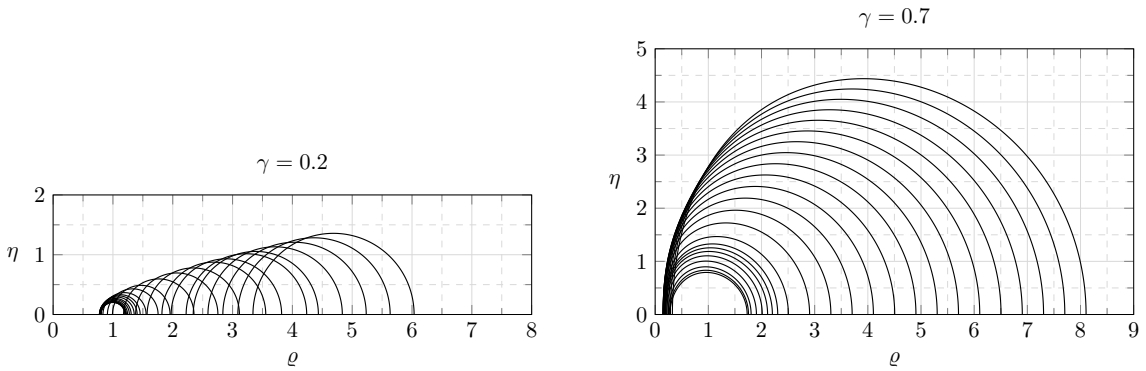


Figure 2. Deformation profiles of the membrane subject to inflation using Ogden energy density function for aspect ratios $\gamma = 0.2$ and $\gamma = 0.7$. The nondimensional coordinates ϱ and η are introduced in (2). Due to symmetry, only the upper half is plotted.

using `fminsearchbnd` function with lower bounds on the guess pair $(\{\eta_\theta(0), P\} > 0)$ in Matlab R2017b. As we capture the desired pair, we use a strong mass-state dependent `ode45` solver in Matlab R2017b to solve the set of equilibrium equations in order to obtain the values of $\varrho, \varrho_\theta, \eta, \eta_\theta$ over the domain $\theta \in [0, \pi]$ which is finely divided into 2000 intervals.

5.1.1. Fundamental solution, deformation profiles, and validation. We plot the inflation profiles of the toroidal membrane for the Ogden model in Figure 2 for the aspect ratios $\gamma = 0.2$ and $\gamma = 0.7$. Similar profiles are obtained for all the models, aspect ratios, and pressure values but not shown here for brevity. It can be seen from Figure 2, left, that for the small aspect ratio ($\gamma = 0.2$), both the inner and the outer ends move outwards while for higher aspect ratio ($\gamma = 0.7$) and Figure 2, right, inner end remains at almost the same position while the outer end moves outwards upon the increase of pressure.

Plots of $\varrho(\pi)$ (inner end) vs. $\varrho(0)$ (outer end) for all the three material models and several aspect ratios $\{\gamma \in (0.2, 0.7)$ for Ogden and Mooney–Rivlin, $\gamma \in (0.2, 0.8)$ for neo-Hookean} are presented in Figure 3. For the Ogden and neo-Hookean models, it is clearly seen that upon the increase of inflation (moving rightwards on the $\varrho(0)$ axis), the inner end first moves slightly inwards and then moves outwards for almost all values of γ . Only for large aspect ratios ($\gamma = 0.7$ for Ogden and $\gamma = 0.7, 0.8$ for neo-Hookean), the inner end undergoes very small changes in its position. This is also expected physically since tori with large γ have very little room for movement of the inner end. The behaviour is different for the two Mooney–Rivlin material models as shown in Figure 3, bottom. For the cases $\{\gamma = 0.2$ to $0.5, \mathfrak{M} = 0.1\}$ and $\{\gamma = 0.2, \mathfrak{M} = 0.3\}$, with an increase in pressure the inner edge moves outwards before moving inwards again for higher inflation. For all other cases, the inner edge moves further inwards monotonically upon increase of pressure.

These considerable differences in behaviours of constitutive models demonstrate the importance of selecting the right model for the material at hand. For example, behaviour of natural rubbers can usually be explained by the three-term Ogden model [1972] while that of certain soft biological tissues can be simulated by the neo-Hookean model [Horný et al. 2006]. Our results for the Mooney–Rivlin model match those presented in [Tamadapu and DasGupta 2014] for $\mathfrak{M} = 0.3, \gamma = 0.2$ and 0.5 cases, and those

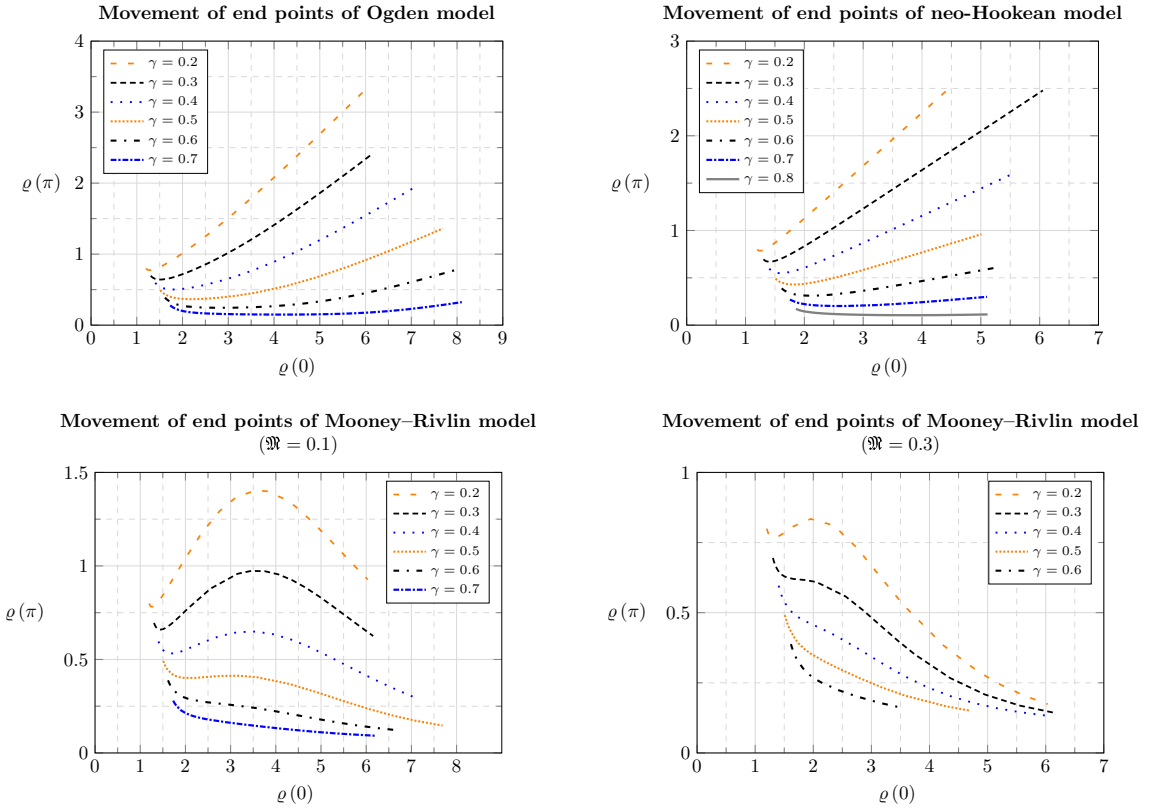


Figure 3. Movement of end points for different hyperelastic constitutive models during inflation of the membrane for various aspect ratios γ . The end $\varrho(0)$ represents the inflation as explained in Section 5.1 and $\varrho(\pi)$ is the inner end of the torus profile.

presented in [Reddy and Saxena 2017] for $\mathfrak{M} = 0.1$, $\gamma = 0.2$ and 0.5 ; thus providing a validation of the formulation and the computations.

5.1.2. Limit point and Cauchy stress. We compute the pressure-deformation and pressure-stress characteristics for all the three material models for the aspect ratios lying in the range $\gamma \in (0.2, 0.8)$. Variation of nondimensional pressure (P) with the relative increase in volume ($\Delta V/V$) of torus for three representative aspect ratios $\gamma = 0.2, 0.4$, and 0.6 is shown in Figure 4. In each of these curves we observe the classical limit point as the point at which pressure stops increasing monotonically. In a pressure controlled experiment, this generally results in a snap-through instability causing uncontrolled increase in membrane’s volume likely leading to failure. However, the states beyond limit point can be reached in a volume controlled experiment.

It is evident from these curves that tori with small aspect ratios γ can sustain much higher pressure values for the same relative increase in volume. This effect is also visible in the limit point pressure P_{lim} plotted in Figure 5. Higher values of γ result in lower values of corresponding P_{lim} . We also note that with comparable values of shear modulus μ used in the computations, Ogden material has the smallest value of P_{lim} followed by neo-Hookean and Mooney–Rivlin materials, respectively. We note that upon

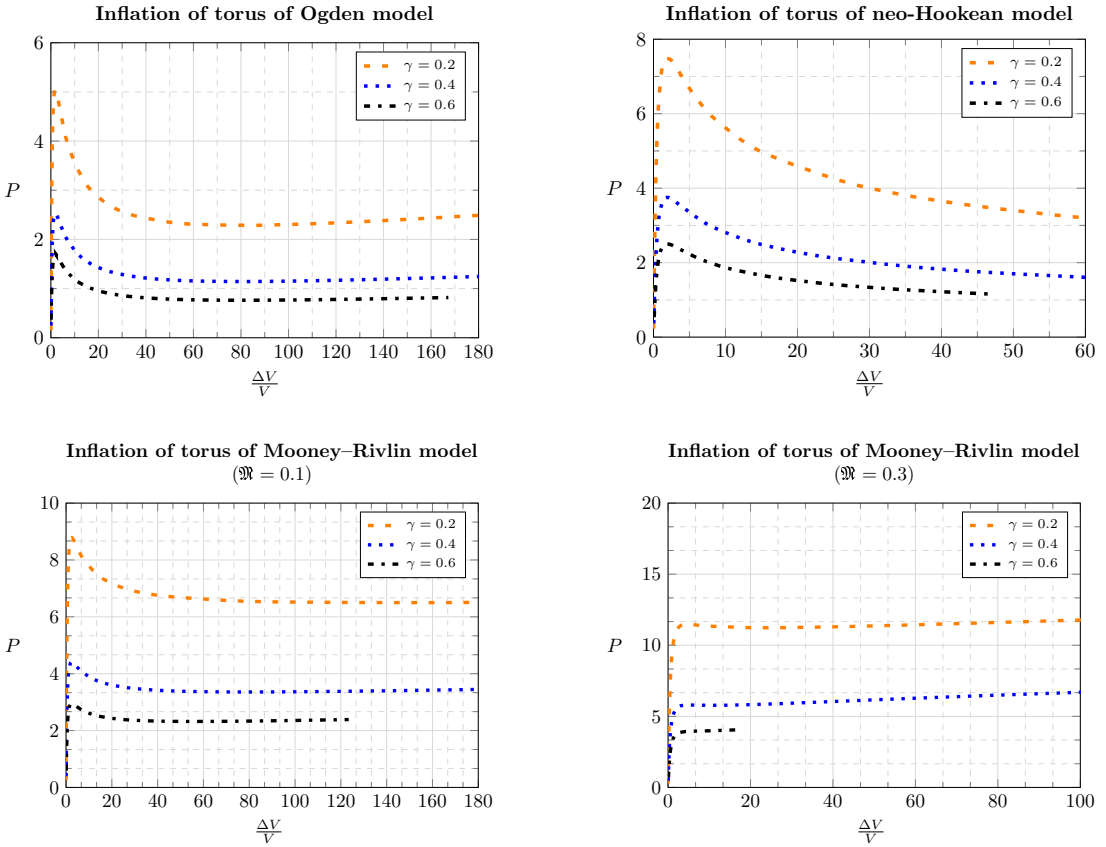


Figure 4. Pressure vs. volume curves for all the three material models for three different aspect ratios $\gamma = 0.2, 0.4, 0.6$.

increasing volume beyond the limit point, there is a consistent decline in pressure for the neo-Hookean model whereas opposite happens for Mooney–Rivlin ($\mathfrak{M} = 0.3, \gamma = 0.6$) case where pressure increases monotonically. In all the other cases (Ogden model, Mooney–Rivlin ($\mathfrak{M} = 0.1$) and Mooney–Rivlin ($\mathfrak{M} = 0.3, \gamma = 0.2, 0.4$)) pressure rises with volume after an initial fall at the limit point.

We also study the variation of Cauchy stresses in the membrane with inflation as computed using (43), (49), and (53). The behaviour is almost similar for all the three models and we plot a few representative results for Ogden model in Figure 6. Variation of the principal stresses $\sigma_{\theta\theta}$ and $\sigma_{\phi\phi}$ at the inner equator ($\theta = \pi$) with the internal pressure is shown. Typically the magnitude of principal stresses along the minor circumference ($\sigma_{\theta\theta}$) is larger than that of the principal stresses along the major circumference ($\sigma_{\phi\phi}$). For most cases, the stresses increase monotonically with inflation, the exception being $\sigma_{\phi\phi}(\theta = \pi)$ at $\gamma = \{0.6, 0.7\}$. Beyond the limit point, the stresses increase rapidly upon slight changes in pressure, likely leading to failure.

We further observe in Figure 6 that $\sigma_{\phi\phi}$ attains a negative value for certain values of pressure for torus with $\gamma = 0.7$. Similar observations are made for the neo-Hookean model ($\gamma = 0.8$) and Mooney–Rivlin model ($\{\mathfrak{M} = 0.1; \gamma = 0.4, 0.5, 0.6, 0.7\}$ and $\{\mathfrak{M} = 0.3; \gamma = 0.2, 0.3, 0.4, 0.5, 0.6\}$) but those results are

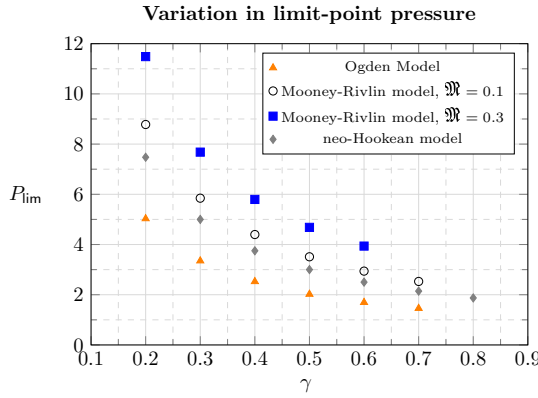


Figure 5. Variation of limit point pressure with aspect ratio for different elastic constitutive models.

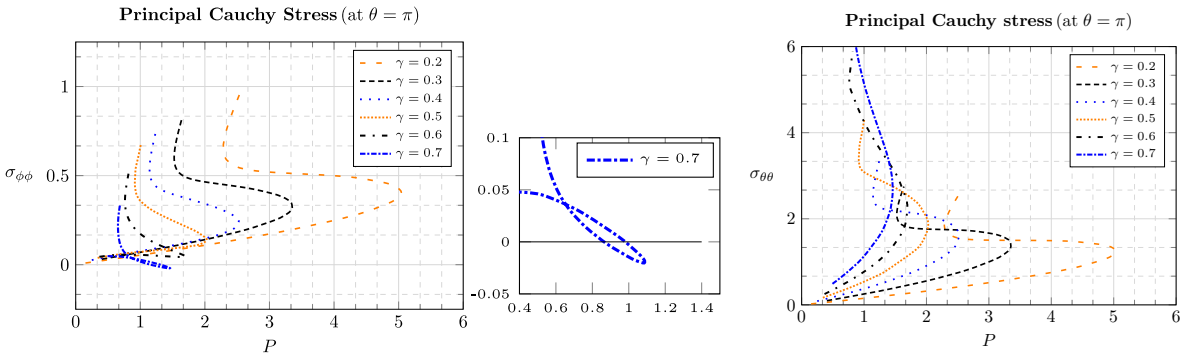


Figure 6. Variation of the principal stresses $\sigma_{\theta\theta}$ and $\sigma_{\phi\phi}$ with pressure at the inner equator ($\theta = \pi$) of the torus for the Ogden material model.

not plotted here for the sake of brevity. Negative values of the principal stress indicate the occurrence of wrinkling instability and this is further explored in Section 5.3.

5.2. Calculation of critical pressure. The fundamental solution obtained for the variables Q_θ and η_θ is used in calculating second order derivatives of Q and η with respect to the variable θ . The values of $Q_{\theta\theta}$ and $\eta_{\theta\theta}$ in each interval are calculated by using forward difference method, i.e., $Q_{\theta\theta_i} = (Q_{\theta_{i+1}} - Q_{\theta_i}) / \Delta\theta$ where $\Delta\theta = \pi/2000$ and $i = 1, 2, \dots, 2000$. The variables (Q, η) and their derivatives are calculated at each θ_i for all the values of pressure during inflation process of a membrane with an aspect ratio γ . These values are substituted in (35) and by changing the values of the mode number n from 1 to 5, we calculate \mathcal{R}_{res} at each θ_i for all the values of pressure and for a given aspect ratio γ . We repeat this process for all the values of $\gamma \in (0.2, 0.8)$ considered in our study for the neo-Hookean material. Zeros of \mathcal{R}_{res} are searched by computing the value of pressure at which it changes sign. Only a change of order ($> \mathcal{O}(10^{-4})$) in the residual value is considered to be admissible to avoid numerical errors; if the value of \mathcal{R}_{res} does not fall in the desired range we do not assign any critical value of pressure for that case. This procedure is repeated for the entire domain $\theta \in [0, \pi]$ and the corresponding critical pressure for the point located

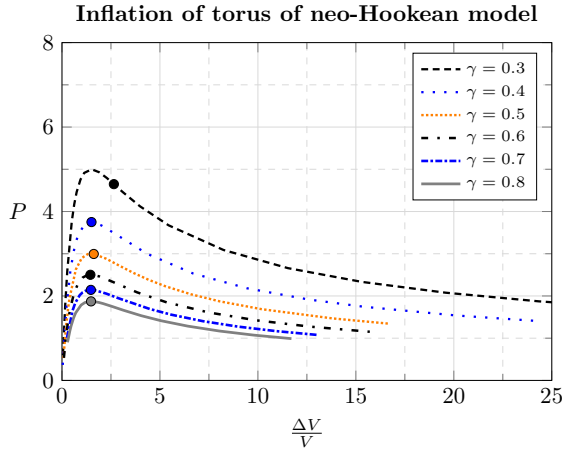


Figure 7. First critical points on the pressure-volume curves for the neo-Hookean model are marked with dots. For $\gamma = 0.3$, critical point is achieved for $n = 2$ and occurs significantly after the limit point, while for all other cases it is achieved at $n = 1$ very close to the limit point.

at θ_i on the membrane is noted. The lowest of all the critical pressure values occurring at or before the limit point for a given aspect ratio is termed as critical point pressure for that membrane under inflation.

Based on our computations, we obtain critical (bifurcation) points for the cases $\{n = 1, \gamma = 0.4, 0.5, 0.6, 0.7, 0.8\}$ and $\{n = 2, \gamma = 0.3\}$. All other cases lead to no solution of (35). The critical point for $\gamma = 0.3$ occurs well after the limit point and although this configuration is difficult to access in a pressure controlled experiment, it can be achieved in a volume or mass controlled experiment [Wang et al. 2017]. For all other γ values, the critical points are very close (albeit not equal) to the limit point. These points are depicted graphically in Figure 7.

5.3. Computation of wrinkling instability. Wrinkling is achieved when the in-plane stress in any direction in the membrane reaches zero. In the negative-stress regions, we use the relaxed form of the strain energy density and the subsequently modified equations in Section 3.2 to recompute the solutions with a method similar to that employed in Section 5.1.

We start with an initial guess value for the location of onset of wrinkling region θ_{wr} taken to be the starting location of the region $\sigma_{\phi\phi} < 0$. We employ standard strain energy density in the region $0 \leq \theta \leq \theta_{wr}$ to calculate the variables $\varrho, \varrho_\theta, \eta,$ and η_θ at θ_{wr} and use these as the initial conditions to determine the solution in the region $\theta_{wr} \leq \theta \leq \pi$ employing the relaxed strain energy density function. Next, we minimise the cost function $[\varrho_\theta(\pi)^2 + \eta(\pi)^2]^{1/2}$ to a sufficiently small quantity ($< \mathcal{O}(10^{-12})$) by using the Nelder–Mead simplex optimisation technique of two variables ($\eta_\theta(0), P$) and determine the variables over the domain $\theta \in [0, \pi]$. Then, we calculate $\lambda_2^2 \lambda_1 - 1$ obtained at θ_{wr} to check if the value is in order of ($< \mathcal{O}(10^{-10})$) and this process is repeated by varying θ_{wr} in the range $(\frac{1}{2}\pi, \pi)$ till we get the desired solution set (λ_1, λ_2) at θ_{wr} , since we observe that both the principal stretch ratio values are greater than one for the points on the boundary in the range $0 \leq \theta \leq \frac{1}{2}\pi$. The coordinate $\theta = \theta_{wr}$ at which $\lambda_2^2 \lambda_1 - 1 < \mathcal{O}(10^{-10})$ represents the starting location of wrinkles on the membrane.

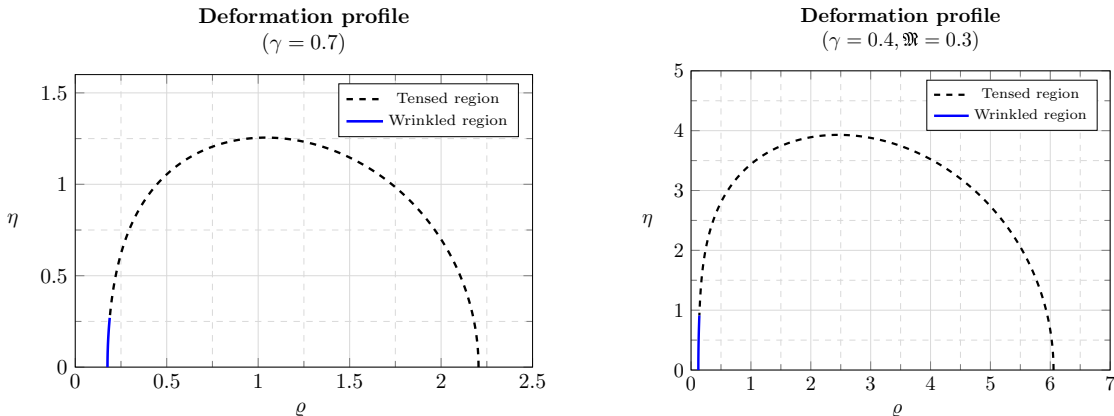


Figure 8. Membrane profiles upon wrinkling computed using relaxed strain energy density. Left: Ogden constitutive model (inflating pressure = 1.46, $\rho(0) = 2.20$). Right: Mooney–Rivlin model (inflating pressure = 7.62, $\rho(0) = 6.05$).

This numerical scheme is implemented in Matlab R2017b. We note that this scheme is an improvement over the traditional case where θ_{wr} would simply be taken as the first point where $\sigma_{\phi\phi} < 0$ based on computations made using the standard energy density function.

Wrinkling analysis is carried out for Ogden material with aspect ratio $\gamma = 0.7$, for Mooney–Rivlin material with $\gamma = 0.4$, $\mathfrak{M} = 0.3$, and for neo-Hookean material with aspect ratio $\gamma = 0.8$ after observing negative $\sigma_{\phi\phi}$ stress values as discussed in Section 5.1.2. We observe that wrinkling occurs only in a small region near the inner equator on the membrane for all the above-mentioned cases whenever $\sigma_{\phi\phi} < 0$. Thus, according to the tension field theory, wrinkling happens along the ϕ direction while the wrinkle lines ought to appear along the θ direction. Membrane profiles upon wrinkling for two cases of Ogden and Mooney–Rivlin models are plotted in Figure 8.

Once the onset of wrinkling is confirmed by observing negative circumferential stress values, we recompute the entire solution using the combination of relaxed and total strain energy densities using the numerical scheme described earlier in this section. We observe that this updated solution (membrane profile and location of wrinkling) is different from the one in which θ_{wr} is obtained using the standard strain energy. Values obtained by both the solutions and relative errors are presented in Table 2. Here $\theta = \theta_{wr}$ is the starting point of wrinkles in the reference configuration. Maximum error in the calculations of θ_{wr} is 0.77% or 1.3° for the Mooney–Rivlin material at the pressure $P = 7.62$. Although the error between these two approaches in this case of toroidal geometry is small, the difference in solutions is still noteworthy and might be more relevant in other constitutive models or membrane geometry.

6. Conclusions

In this work we have presented new analysis and results in the study of free inflation of a nonlinear hyperelastic toroidal membrane. To analyse the deformation behaviour and instabilities in free inflation of a torus under a hydrostatic pressure, toroidal membranes made of three materials (Ogden, Mooney–Rivlin, and neo-Hookean) are considered and a comparative study is conducted amongst them. We observe

| model | | | standard energy | relaxed energy | error % |
|---|--------------|------|-----------------|----------------|---------|
| | $\varrho(0)$ | P | density | density | |
| Ogden ($\gamma = 0.7$) | 2.01 | 1.41 | 173.97° | 172.98° | 0.57 |
| | 2.20 | 1.46 | 173.07° | 171.81° | 0.73 |
| Mooney–Rivlin ($\gamma = 0.4, \mathfrak{M} = 0.3$) | 5.55 | 7.23 | 176.13° | 175.41° | 0.41 |
| | 6.05 | 7.62 | 174.42° | 173.07° | 0.77 |
| neo-Hookean ($\gamma = 0.8$) | 2.21 | 1.84 | 175.41° | 174.60° | 0.46 |
| | 2.31 | 1.87 | 175.41° | 174.60° | 0.46 |

Table 2. Error in the prediction of the parameter θ_{wr} by standard strain energy density function.

strain-hardening behaviour in Ogden and Mooney–Rivlin material models after the limit point pressure. For the neo-Hookean model bifurcation of solution occurs well post limit point for $\gamma = 0.3$ corresponding to the second mode, and very close to the limit point for all other aspect ratios for the first mode.

We notice that limit point pressure decreases with increase in aspect ratio and increases with increase in stiffness of the membrane. We also notice that for Mooney–Rivlin model with higher aspect ratio and a stiffer material, nondimensional pressure increases monotonically with inflation. In the compressive stress regions, we use the concept of relaxed strain energy density to study wrinkling behaviour and we observe differences between the wrinkled configuration predicted by standard strain energy density and its relaxed form.

Based on our results on critical point bifurcation and wrinkling, it can be claimed that the predicted behaviour of membrane in Figure 4 and Figure 6 for large volume cases is most likely inaccurate. The fundamental solution does not hold for the postinstability regime and a recalculation of configuration/ stress/ pressure needs to be performed. This postbuckling analysis to understand membrane’s behaviour will be undertaken as future work.

Appendix: Matrix coefficients of governing equations for various constitutive models

A.1. Coefficients for Ogden model. For Ogden constitutive model, the governing equation (8) gives

$$\sum_{j=1}^3 \frac{\mu_j}{\lambda_1^{\alpha_j+3} \lambda_2^{\alpha_j+1} \gamma^{2\alpha_j+2} R^{2\alpha_j+2} [\varrho_\theta^2 + \eta_\theta^2]^{3/2}} [\widehat{A}_j \varrho_{\theta\theta} + \widehat{B}_j \eta_{\theta\theta} + \widehat{C}_j] + \left[\frac{\widehat{P}R_b}{T} \right] \varrho \eta_\theta = 0, \tag{36}$$

while the governing equation (9) results in

$$\sum_{j=1}^3 \frac{\mu_j}{\lambda_1^{\alpha_j+3} \lambda_2^{\alpha_j+1} \gamma^{2\alpha_j+2} R^{2\alpha_j+2} [\varrho_\theta^2 + \eta_\theta^2]^{3/2}} [\widehat{D}_j \varrho_{\theta\theta} + \widehat{E}_j \eta_{\theta\theta} + \widehat{F}_j] - \left[\frac{\widehat{P}R_b}{T} \right] \varrho \varrho_\theta = 0, \tag{37}$$

where

$$\begin{aligned} \widehat{A}_j = & [[\alpha_j - 1][\varrho_\theta^2 + \eta_\theta^2]^{\alpha_j} \varrho^{\alpha_j} R^{\alpha_j} + [\alpha_j + 1]\gamma^{2\alpha_j} R^{2\alpha_j}] \varrho_\theta^2 [\varrho_\theta^2 + \eta_\theta^2] \varrho R^2 \\ & + [[\varrho_\theta^2 + \eta_\theta^2]^{\alpha_j} \varrho^{\alpha_j} R^{\alpha_j} - \gamma^{2\alpha_j} R^{2\alpha_j}] \eta_\theta^2 [\varrho_\theta^2 + \eta_\theta^2] \varrho R^2, \end{aligned}$$

$$\begin{aligned} \widehat{B}_j &= [\alpha_j - 1][\varrho_\theta^2 + \eta_\theta^2]^{\alpha_j} \varrho^{\alpha_j} R^{\alpha_j} + [\alpha_j + 1]\gamma^{2\alpha_j} R^{2\alpha_j} \varrho_\theta \eta_\theta [\varrho_\theta^2 + \eta_\theta^2] \varrho R^2 \\ &\quad - [[\varrho_\theta^2 + \eta_\theta^2]^{\alpha_j} \varrho^{\alpha_j} R^{\alpha_j} - \gamma^{2\alpha_j} R^{2\alpha_j}] \varrho_\theta \eta_\theta [\varrho_\theta^2 + \eta_\theta^2] \varrho R^2, \\ \widehat{C}_j &= \alpha_j [\varrho_\theta R + \varrho \gamma \sin \theta] \varrho_\theta [\varrho_\theta^2 + \eta_\theta^2]^2 \gamma^{2\alpha_j} R^{2\alpha_j+1} \\ &\quad - [[\varrho_\theta^2 + \eta_\theta^2]^{\alpha_j} \varrho^{\alpha_j} R^{\alpha_j} - \gamma^{2\alpha_j} R^{2\alpha_j}] \varrho_\theta \varrho [\varrho_\theta^2 + \eta_\theta^2]^2 \gamma R \sin \theta \\ &\quad - [[\varrho_\theta^2 + \eta_\theta^2]^{\alpha_j/2} \varrho^{2\alpha_j} \gamma^{\alpha_j} - \gamma^{2\alpha_j} R^{2\alpha_j}] [\varrho_\theta^2 + \eta_\theta^2]^3 R^2, \end{aligned} \tag{38}$$

and

$$\begin{aligned} \widehat{D}_j &= [\alpha_j - 1][\varrho_\theta^2 + \eta_\theta^2]^{\alpha_j} \varrho^{\alpha_j} R^{\alpha_j} + [\alpha_j + 1]\gamma^{2\alpha_j} R^{2\alpha_j} \varrho_\theta \eta_\theta [\varrho_\theta^2 + \eta_\theta^2] \varrho R^2 \\ &\quad - [[\varrho_\theta^2 + \eta_\theta^2]^{\alpha_j} \varrho^{\alpha_j} R^{\alpha_j} - \gamma^{2\alpha_j} R^{2\alpha_j}] \varrho_\theta \eta_\theta [\varrho_\theta^2 + \eta_\theta^2] \varrho R^2, \\ \widehat{E}_j &= [\alpha_j - 1][\varrho_\theta^2 + \eta_\theta^2]^{\alpha_j} \varrho^{\alpha_j} R^{\alpha_j} + [\alpha_j + 1]\gamma^{2\alpha_j} R^{2\alpha_j} \eta_\theta^2 [\varrho_\theta^2 + \eta_\theta^2] \varrho R^2 \\ &\quad + [[\varrho_\theta^2 + \eta_\theta^2]^{\alpha_j} \varrho^{\alpha_j} R^{\alpha_j} - \gamma^{2\alpha_j} R^{2\alpha_j}] \varrho_\theta^2 [\varrho_\theta^2 + \eta_\theta^2] \varrho R^2, \\ \widehat{F}_j &= \alpha_j [\varrho_\theta R + \varrho \gamma \sin \theta] \eta_\theta [\varrho_\theta^2 + \eta_\theta^2]^2 \gamma^{2\alpha_j} R^{2\alpha_j+1} \\ &\quad - [[\varrho_\theta^2 + \eta_\theta^2]^{\alpha_j} \varrho^{\alpha_j} R^{\alpha_j} - \gamma^{2\alpha_j} R^{2\alpha_j}] \varrho_\theta \eta_\theta [\varrho_\theta^2 + \eta_\theta^2]^2 \gamma R \sin \theta. \end{aligned} \tag{39}$$

The components of matrices in (14) for the Ogden energy density are given by

$$\begin{aligned} S_{22} &= \mu_1^* [\mathcal{U}_1 R^2 [\mathcal{U}_2^2 + \mathcal{U}_4^2] [[\mathcal{S}^1] \mathcal{U}_2^2 + [\mathcal{S}^2] \mathcal{U}_4^2]] \lambda_1^{\alpha_2+\alpha_3+6} \lambda_2^{\alpha_2+\alpha_3+2} \gamma^{2\alpha_2+2\alpha_3+4} R^{2\alpha_2+2\alpha_3+4} \\ &\quad + \mu_2^* [\mathcal{U}_1 R^2 [\mathcal{U}_2^2 + \mathcal{U}_4^2] [[\mathcal{S}^3] \mathcal{U}_2^2 + [\mathcal{S}^4] \mathcal{U}_4^2]] \lambda_1^{\alpha_1+\alpha_3+6} \lambda_2^{\alpha_1+\alpha_3+2} \gamma^{2\alpha_1+2\alpha_3+4} R^{2\alpha_1+2\alpha_3+4} \\ &\quad + \mu_3^* [\mathcal{U}_1 R^2 [\mathcal{U}_2^2 + \mathcal{U}_4^2] [[\mathcal{S}^5] \mathcal{U}_2^2 + [\mathcal{S}^6] \mathcal{U}_4^2]] \lambda_1^{\alpha_1+\alpha_2+6} \lambda_2^{\alpha_1+\alpha_2+2} \gamma^{2\alpha_1+2\alpha_2+4} R^{2\alpha_1+2\alpha_2+4}, \\ S_{24} &= \mu_1^* [\mathcal{U}_1 R^2 [\mathcal{U}_2^2 + \mathcal{U}_4^2] [[\mathcal{S}^1] \mathcal{U}_2 \mathcal{U}_4 - [\mathcal{S}^2] \mathcal{U}_2 \mathcal{U}_4]] \lambda_1^{\alpha_2+\alpha_3+6} \lambda_2^{\alpha_2+\alpha_3+2} \gamma^{2\alpha_2+2\alpha_3+4} R^{2\alpha_2+2\alpha_3+4} \\ &\quad + \mu_2^* [\mathcal{U}_1 R^2 [\mathcal{U}_2^2 + \mathcal{U}_4^2] [[\mathcal{S}^3] \mathcal{U}_2 \mathcal{U}_4 - [\mathcal{S}^4] \mathcal{U}_2 \mathcal{U}_4]] \lambda_1^{\alpha_1+\alpha_3+6} \lambda_2^{\alpha_1+\alpha_3+2} \gamma^{2\alpha_1+2\alpha_3+4} R^{2\alpha_1+2\alpha_3+4} \\ &\quad + \mu_3^* [\mathcal{U}_1 R^2 [\mathcal{U}_2^2 + \mathcal{U}_4^2] [[\mathcal{S}^5] \mathcal{U}_2 \mathcal{U}_4 - [\mathcal{S}^6] \mathcal{U}_2 \mathcal{U}_4]] \lambda_1^{\alpha_1+\alpha_2+6} \lambda_2^{\alpha_1+\alpha_2+2} \gamma^{2\alpha_1+2\alpha_2+4} R^{2\alpha_1+2\alpha_2+4}, \\ S_{42} &= \mu_1^* [\mathcal{U}_1 R^2 [\mathcal{U}_2^2 + \mathcal{U}_4^2] [[\mathcal{S}^1] \mathcal{U}_2 \mathcal{U}_4 - [\mathcal{S}^2] \mathcal{U}_2 \mathcal{U}_4]] \lambda_1^{\alpha_2+\alpha_3+6} \lambda_2^{\alpha_2+\alpha_3+2} \gamma^{2\alpha_2+2\alpha_3+4} R^{2\alpha_2+2\alpha_3+4} \\ &\quad + \mu_2^* [\mathcal{U}_1 R^2 [\mathcal{U}_2^2 + \mathcal{U}_4^2] [[\mathcal{S}^3] \mathcal{U}_2 \mathcal{U}_4 - [\mathcal{S}^4] \mathcal{U}_2 \mathcal{U}_4]] \lambda_1^{\alpha_1+\alpha_3+6} \lambda_2^{\alpha_1+\alpha_3+2} \gamma^{2\alpha_1+2\alpha_3+4} R^{2\alpha_1+2\alpha_3+4} \\ &\quad + \mu_3^* [\mathcal{U}_1 R^2 [\mathcal{U}_2^2 + \mathcal{U}_4^2] [[\mathcal{S}^5] \mathcal{U}_2 \mathcal{U}_4 - [\mathcal{S}^6] \mathcal{U}_2 \mathcal{U}_4]] \lambda_1^{\alpha_1+\alpha_2+6} \lambda_2^{\alpha_1+\alpha_2+2} \gamma^{2\alpha_1+2\alpha_2+4} R^{2\alpha_1+2\alpha_2+4}, \\ S_{44} &= \mu_1^* [\mathcal{U}_1 R^2 [\mathcal{U}_2^2 + \mathcal{U}_4^2] [[\mathcal{S}^1] \mathcal{U}_4^2 + [\mathcal{S}^2] \mathcal{U}_2^2]] \lambda_1^{\alpha_2+\alpha_3+6} \lambda_2^{\alpha_2+\alpha_3+2} \gamma^{2\alpha_2+2\alpha_3+4} R^{2\alpha_2+2\alpha_3+4} \\ &\quad + \mu_2^* [\mathcal{U}_1 R^2 [\mathcal{U}_2^2 + \mathcal{U}_4^2] [[\mathcal{S}^3] \mathcal{U}_4^2 + [\mathcal{S}^4] \mathcal{U}_2^2]] \lambda_1^{\alpha_1+\alpha_3+6} \lambda_2^{\alpha_1+\alpha_3+2} \gamma^{2\alpha_1+2\alpha_3+4} R^{2\alpha_1+2\alpha_3+4} \\ &\quad + \mu_3^* [\mathcal{U}_1 R^2 [\mathcal{U}_2^2 + \mathcal{U}_4^2] [[\mathcal{S}^5] \mathcal{U}_4^2 + [\mathcal{S}^6] \mathcal{U}_2^2]] \lambda_1^{\alpha_1+\alpha_2+6} \lambda_2^{\alpha_1+\alpha_2+2} \gamma^{2\alpha_1+2\alpha_2+4} R^{2\alpha_1+2\alpha_2+4}, \end{aligned} \tag{40}$$

and

$$\begin{aligned} \mathcal{V}_1 &= \mu_1^* [[\mathcal{V}^2] \mathcal{U}_1 \mathcal{U}_2 [\mathcal{U}_2^2 + \mathcal{U}_4^2]^2 \gamma R \sin \theta + [\mathcal{V}^7] [\mathcal{U}_2^2 + \mathcal{U}_4^2]^3 R^2] \lambda_1^{\alpha_2+\alpha_3+6} \lambda_2^{\alpha_2+\alpha_3+2} \gamma^{2\alpha_2+2\alpha_3+4} R^{2\alpha_2+2\alpha_3+4} \\ &\quad - \mu_1^* [[\mathcal{V}^1] \mathcal{U}_2 [\mathcal{U}_2^2 + \mathcal{U}_4^2]^2] \lambda_1^{\alpha_2+\alpha_3+6} \lambda_2^{\alpha_2+\alpha_3+2} \gamma^{2\alpha_2+2\alpha_3+4} R^{2\alpha_2+2\alpha_3+4} \\ &\quad + \mu_2^* [[\mathcal{V}^4] \mathcal{U}_1 \mathcal{U}_2 [\mathcal{U}_2^2 + \mathcal{U}_4^2]^2 \gamma R \sin \theta + [\mathcal{V}^8] [\mathcal{U}_2^2 + \mathcal{U}_4^2]^3 R^2] \lambda_1^{\alpha_1+\alpha_3+6} \lambda_2^{\alpha_1+\alpha_3+2} \gamma^{2\alpha_1+2\alpha_3+4} R^{2\alpha_1+2\alpha_3+4} \\ &\quad - \mu_2^* [[\mathcal{V}^3] \mathcal{U}_2 [\mathcal{U}_2^2 + \mathcal{U}_4^2]^2] \lambda_1^{\alpha_1+\alpha_3+6} \lambda_2^{\alpha_1+\alpha_3+2} \gamma^{2\alpha_1+2\alpha_3+4} R^{2\alpha_1+2\alpha_3+4} \end{aligned}$$

$$\begin{aligned}
 & + \mu_3^* [\nu^6] \mathcal{U}_1 \mathcal{U}_2 [\mathcal{U}_2^2 + \mathcal{U}_4^2]^2 \gamma R \sin \theta + [\nu^9] [\mathcal{U}_2^2 + \mathcal{U}_4^2]^3 R^2 \lambda_1^{\alpha_1 + \alpha_2 + 6} \lambda_2^{\alpha_1 + \alpha_2 + 2} \gamma^{2\alpha_1 + 2\alpha_2 + 4} R^{2\alpha_1 + 2\alpha_2 + 4} \\
 & - \mu_3^* [\nu^5] \mathcal{U}_2 [\mathcal{U}_2^2 + \mathcal{U}_4^2]^2 \lambda_1^{\alpha_1 + \alpha_2 + 6} \lambda_2^{\alpha_1 + \alpha_2 + 2} \gamma^{2\alpha_1 + 2\alpha_2 + 4} R^{2\alpha_1 + 2\alpha_2 + 4} \\
 & - \frac{1}{2} \mu_1^* P \mathcal{U}_1 \mathcal{U}_4 [\mathcal{U}_2^2 + \mathcal{U}_4^2]^{3/2} \lambda_1^{\alpha_1 + \alpha_2 + \alpha_3 + 9} \lambda_2^{\alpha_1 + \alpha_2 + \alpha_3 + 3} \gamma^{2\alpha_1 + 2\alpha_2 + 2\alpha_3 + 6} R^{2\alpha_1 + 2\alpha_2 + 2\alpha_3 + 6}, \\
 \mathcal{V}_2 = & \mu_1^* [\nu^2] \mathcal{U}_1 \mathcal{U}_4 [\mathcal{U}_2^2 + \mathcal{U}_4^2]^2 \gamma R \sin \theta \lambda_1^{\alpha_2 + \alpha_3 + 6} \lambda_2^{\alpha_2 + \alpha_3 + 2} \gamma^{2\alpha_2 + 2\alpha_3 + 4} R^{2\alpha_2 + 2\alpha_3 + 4} \\
 & - \mu_1^* [\nu^1] \mathcal{U}_4 [\mathcal{U}_2^2 + \mathcal{U}_4^2]^2 \lambda_1^{\alpha_2 + \alpha_3 + 6} \lambda_2^{\alpha_2 + \alpha_3 + 2} \gamma^{2\alpha_2 + 2\alpha_3 + 4} R^{2\alpha_2 + 2\alpha_3 + 4} \\
 & + \mu_2^* [\nu^4] \mathcal{U}_1 \mathcal{U}_4 [\mathcal{U}_2^2 + \mathcal{U}_4^2]^2 \gamma R \sin \theta \lambda_1^{\alpha_1 + \alpha_3 + 6} \lambda_2^{\alpha_1 + \alpha_3 + 2} \gamma^{2\alpha_1 + 2\alpha_3 + 4} R^{2\alpha_1 + 2\alpha_3 + 4} \\
 & - \mu_2^* [\nu^3] \mathcal{U}_4 [\mathcal{U}_2^2 + \mathcal{U}_4^2]^2 \lambda_1^{\alpha_1 + \alpha_3 + 6} \lambda_2^{\alpha_1 + \alpha_3 + 2} \gamma^{2\alpha_1 + 2\alpha_3 + 4} R^{2\alpha_1 + 2\alpha_3 + 4} \\
 & + \mu_3^* [\nu^6] \mathcal{U}_1 \mathcal{U}_4 [\mathcal{U}_2^2 + \mathcal{U}_4^2]^2 \gamma R \sin \theta \lambda_1^{\alpha_1 + \alpha_2 + 6} \lambda_2^{\alpha_1 + \alpha_2 + 2} \gamma^{2\alpha_1 + 2\alpha_2 + 4} R^{2\alpha_1 + 2\alpha_2 + 4} \\
 & - \mu_3^* [\nu^5] \mathcal{U}_4 [\mathcal{U}_2^2 + \mathcal{U}_4^2]^2 \lambda_1^{\alpha_1 + \alpha_2 + 6} \lambda_2^{\alpha_1 + \alpha_2 + 2} \gamma^{2\alpha_1 + 2\alpha_2 + 4} R^{2\alpha_1 + 2\alpha_2 + 4} \\
 & + \frac{1}{2} \mu_1^* P \mathcal{U}_1 \mathcal{U}_2 [\mathcal{U}_2^2 + \mathcal{U}_4^2]^{3/2} \lambda_1^{\alpha_1 + \alpha_2 + \alpha_3 + 9} \lambda_2^{\alpha_1 + \alpha_2 + \alpha_3 + 3} \gamma^{2\alpha_1 + 2\alpha_2 + 2\alpha_3 + 6} R^{2\alpha_1 + 2\alpha_2 + 2\alpha_3 + 6}, \tag{41}
 \end{aligned}$$

along with

$$\begin{aligned}
 \mathcal{S}^1 &= [\alpha_1 - 1] [\mathcal{U}_2^2 + \mathcal{U}_4^2]^{\alpha_1} \mathcal{U}_1^{\alpha_1} R^{\alpha_1} + [\alpha_1 + 1] \gamma^{2\alpha_1} R^{2\alpha_1}, & \mathcal{S}^2 &= [\mathcal{U}_2^2 + \mathcal{U}_4^2]^{\alpha_1} \mathcal{U}_1^{\alpha_1} R^{\alpha_1} - \gamma^{2\alpha_1} R^{2\alpha_1}, \\
 \mathcal{S}^3 &= [\alpha_2 - 1] [\mathcal{U}_2^2 + \mathcal{U}_4^2]^{\alpha_2} \mathcal{U}_1^{\alpha_2} R^{\alpha_2} + [\alpha_2 + 1] \gamma^{2\alpha_2} R^{2\alpha_2}, & \mathcal{S}^4 &= [\mathcal{U}_2^2 + \mathcal{U}_4^2]^{\alpha_2} \mathcal{U}_1^{\alpha_2} R^{\alpha_2} - \gamma^{2\alpha_2} R^{2\alpha_2}, \\
 \mathcal{S}^5 &= [\alpha_3 - 1] [\mathcal{U}_2^2 + \mathcal{U}_4^2]^{\alpha_3} \mathcal{U}_1^{\alpha_3} R^{\alpha_3} + [\alpha_3 + 1] \gamma^{2\alpha_3} R^{2\alpha_3}, & \mathcal{S}^6 &= [\mathcal{U}_2^2 + \mathcal{U}_4^2]^{\alpha_3} \mathcal{U}_1^{\alpha_3} R^{\alpha_3} - \gamma^{2\alpha_3} R^{2\alpha_3}, \\
 \mathcal{V}^1 &= \alpha_1 [\mathcal{U}_2 R + \mathcal{U}_1 \gamma \sin \theta] \gamma^{2\alpha_1} R^{2\alpha_1 + 1}, & \mathcal{V}^2 &= [\mathcal{U}_2^2 + \mathcal{U}_4^2]^{\alpha_1} \mathcal{U}_1^{\alpha_1} R^{\alpha_1} - \gamma^{2\alpha_1} R^{2\alpha_1}, \\
 \mathcal{V}^3 &= \alpha_2 [\mathcal{U}_2 R + \mathcal{U}_1 \gamma \sin \theta] \gamma^{2\alpha_2} R^{2\alpha_2 + 1}, & \mathcal{V}^4 &= [\mathcal{U}_2^2 + \mathcal{U}_4^2]^{\alpha_2} \mathcal{U}_1^{\alpha_2} R^{\alpha_2} - \gamma^{2\alpha_2} R^{2\alpha_2}, \\
 \mathcal{V}^5 &= \alpha_3 [\mathcal{U}_2 R + \mathcal{U}_1 \gamma \sin \theta] \gamma^{2\alpha_3} R^{2\alpha_3 + 1}, & \mathcal{V}^6 &= [\mathcal{U}_2^2 + \mathcal{U}_4^2]^{\alpha_3} \mathcal{U}_1^{\alpha_3} R^{\alpha_3} - \gamma^{2\alpha_3} R^{2\alpha_3}, \\
 \mathcal{V}^7 &= [\mathcal{U}_2^2 + \mathcal{U}_4^2]^{\alpha_1/2} \mathcal{U}_1^{2\alpha_1} \gamma^{\alpha_1} - \gamma^{2\alpha_1} R^{2\alpha_1}, & \mathcal{V}^8 &= [\mathcal{U}_2^2 + \mathcal{U}_4^2]^{\alpha_2/2} \mathcal{U}_1^{2\alpha_2} \gamma^{\alpha_2} - \gamma^{2\alpha_2} R^{2\alpha_2}, \\
 \mathcal{V}^9 &= [\mathcal{U}_2^2 + \mathcal{U}_4^2]^{\alpha_3/2} \mathcal{U}_1^{2\alpha_3} \gamma^{\alpha_3} - \gamma^{2\alpha_3} R^{2\alpha_3}, \\
 P &= \frac{2\widehat{P}R_b}{\mu_1 T}. \tag{42}
 \end{aligned}$$

Nondimensional principal Cauchy stresses in the θ - and ϕ -directions are computed as

$$\sigma_{\theta\theta} = \left[\frac{\lambda_3 \alpha_1}{\mu_1^*} \right] \left[\sum_{j=1}^3 \mu_j^* \lambda_1^{\alpha_j} - \sum_{j=1}^3 \mu_j^* \lambda_3^{\alpha_j} \right], \quad \sigma_{\phi\phi} = \left[\frac{\lambda_3 \alpha_1}{\mu_1^*} \right] \left[\sum_{j=1}^3 \mu_j^* \lambda_2^{\alpha_j} - \sum_{j=1}^3 \mu_j^* \lambda_3^{\alpha_j} \right]. \tag{43}$$

A.2. Coefficients for Mooney–Rivlin model. The components of matrices in (14) for the Mooney–Rivlin energy density are given by

$$\begin{aligned}
 \mathcal{S}_{22} &= [\mathcal{U}_1 R^2 [\mathcal{U}_2^2 + \mathcal{U}_4^2] [[\mathcal{S}_m^1] \mathcal{U}_2^2 + [\mathcal{S}_m^2] \mathcal{U}_4^2]] \lambda_1^4 \\
 &\quad - \mathfrak{M} [\mathcal{U}_1 R^2 [\mathcal{U}_2^2 + \mathcal{U}_4^2] [[\mathcal{S}_m^3] \mathcal{U}_2^2 + [\mathcal{S}_m^4] \mathcal{U}_4^2]] \lambda_1^8 \lambda_2^4 \gamma^8 R^8, \\
 \mathcal{S}_{24} &= [\mathcal{U}_1 R^2 [\mathcal{U}_2^2 + \mathcal{U}_4^2] [[\mathcal{S}_m^1] \mathcal{U}_2 \mathcal{U}_4 - [\mathcal{S}_m^2] \mathcal{U}_2 \mathcal{U}_4]] \lambda_1^4 \\
 &\quad - \mathfrak{M} [\mathcal{U}_1 R^2 [\mathcal{U}_2^2 + \mathcal{U}_4^2] [[\mathcal{S}_m^3] \mathcal{U}_2 \mathcal{U}_4 - [\mathcal{S}_m^4] \mathcal{U}_2 \mathcal{U}_4]] \lambda_1^8 \lambda_2^4 \gamma^8 R^8,
 \end{aligned}$$

$$\begin{aligned} \mathcal{S}_{42} = \mathcal{S}_{24}, \mathcal{S}_{44} = & [\mathcal{U}_1 R^2 [\mathcal{U}_2^2 + \mathcal{U}_4^2] [\mathcal{S}_m^1 \mathcal{U}_4^2 + \mathcal{S}_m^2 \mathcal{U}_2^2]] \lambda_1^4 \\ & - \mathfrak{M} [\mathcal{U}_1 R^2 [\mathcal{U}_2^2 + \mathcal{U}_4^2] [\mathcal{S}_m^3 \mathcal{U}_4^2 + \mathcal{S}_m^4 \mathcal{U}_2^2]] \lambda_1^8 \lambda_2^4 \gamma^8 R^8, \end{aligned} \quad (44)$$

and

$$\begin{aligned} \mathcal{V}_1 = & [\mathcal{V}_m^2 \mathcal{U}_1 \mathcal{U}_2 [\mathcal{U}_2^2 + \mathcal{U}_4^2]^2 \gamma R \sin \theta + \mathcal{V}_m^5] [\mathcal{U}_2^2 + \mathcal{U}_4^2]^3 R^2] \lambda_1^4 - [\mathcal{V}_m^1 \mathcal{U}_2 [\mathcal{U}_2^2 + \mathcal{U}_4^2]^2] \lambda_1^4 \\ & - \mathfrak{M} [\mathcal{V}_m^4 \mathcal{U}_1 \mathcal{U}_2 [\mathcal{U}_2^2 + \mathcal{U}_4^2]^2 \gamma R \sin \theta + \mathcal{V}_m^6] [\mathcal{U}_2^2 + \mathcal{U}_4^2]^3 R^2] \lambda_1^8 \lambda_2^4 \gamma^8 R^8 \\ & + \mathfrak{M} [\mathcal{V}_m^3 \mathcal{U}_2 [\mathcal{U}_2^2 + \mathcal{U}_4^2]^2] \lambda_1^8 \lambda_2^4 \gamma^8 R^8 - \frac{1}{2} P \mathcal{U}_1 \mathcal{U}_4 [\mathcal{U}_2^2 + \mathcal{U}_4^2]^{3/2} \lambda_1^9 \lambda_2^3 \gamma^6 R^6, \\ \mathcal{V}_2 = & [\mathcal{V}_m^2 \mathcal{U}_1 \mathcal{U}_4 [\mathcal{U}_2^2 + \mathcal{U}_4^2]^2 \gamma R \sin \theta] \lambda_1^4 - [\mathcal{V}_m^1 \mathcal{U}_4 [\mathcal{U}_2^2 + \mathcal{U}_4^2]^2] \lambda_1^4 \\ & - \mathfrak{M} [\mathcal{V}_m^4 \mathcal{U}_1 \mathcal{U}_4 [\mathcal{U}_2^2 + \mathcal{U}_4^2]^2 \gamma R \sin \theta] \lambda_1^8 \lambda_2^4 \gamma^8 R^8 \\ & + \mathfrak{M} [\mathcal{V}_m^3 \mathcal{U}_4 [\mathcal{U}_2^2 + \mathcal{U}_4^2]^2] \lambda_1^8 \lambda_2^4 \gamma^8 R^8 + \frac{1}{2} P \mathcal{U}_1 \mathcal{U}_2 [\mathcal{U}_2^2 + \mathcal{U}_4^2]^{3/2} \lambda_1^9 \lambda_2^3 \gamma^6 R^6, \end{aligned} \quad (45)$$

along with

$$\begin{aligned} \mathcal{S}_m^1 = & [\mathcal{U}_2^2 + \mathcal{U}_4^2]^2 \mathcal{U}_1^2 R^2 + 3\gamma^4 R^4, & \mathcal{S}_m^2 = & [\mathcal{U}_2^2 + \mathcal{U}_4^2]^2 \mathcal{U}_1^2 R^2 - \gamma^4 R^4, \\ \mathcal{S}_m^3 = & -3[\mathcal{U}_2^2 + \mathcal{U}_4^2]^{-2} \mathcal{U}_1^{-2} R^{-2} - \gamma^{-4} R^{-4}, & \mathcal{S}_m^4 = & [\mathcal{U}_2^2 + \mathcal{U}_4^2]^{-2} \mathcal{U}_1^{-2} R^{-2} - \gamma^{-4} R^{-4}, \end{aligned} \quad (46)$$

$$\begin{aligned} \mathcal{V}_m^1 = & 2[\mathcal{U}_2 R + \mathcal{U}_1 \gamma \sin \theta] \gamma^4 R^5, & \mathcal{V}_m^2 = & [\mathcal{U}_2^2 + \mathcal{U}_4^2]^2 \mathcal{U}_1^2 R^2 - \gamma^4 R^4, \\ \mathcal{V}_m^3 = & -2[\mathcal{U}_2 R + \mathcal{U}_1 \gamma \sin \theta] \gamma^{-4} R^{-3}, & \mathcal{V}_m^4 = & [\mathcal{U}_2^2 + \mathcal{U}_4^2]^{-2} \mathcal{U}_1^{-2} R^{-2} - \gamma^{-4} R^{-4}, \\ \mathcal{V}_m^5 = & [\mathcal{U}_2^2 + \mathcal{U}_4^2] \mathcal{U}_1^4 \gamma^2 - \gamma^4 R^4, & \mathcal{V}_m^6 = & [\mathcal{U}_2^2 + \mathcal{U}_4^2]^{-1} \mathcal{U}_1^{-4} \gamma^{-2} - \gamma^{-4} R^{-4}, \end{aligned} \quad (47)$$

$$P = \frac{\widehat{P} R_b}{\frac{1}{2} \mu_1 T}, \quad \mathfrak{M} = -\frac{\mu_2}{\mu_1}. \quad (48)$$

Nondimensional principal Cauchy stresses in the θ - and ϕ -directions are computed as

$$\sigma_{\theta\theta} = 2 \left[\frac{\lambda_1}{\lambda_2} - \frac{1}{\lambda_1^3 \lambda_2^3} \right] [1 + \mathfrak{M} \lambda_2^2], \quad \sigma_{\phi\phi} = 2 \left[\frac{\lambda_2}{\lambda_1} - \frac{1}{\lambda_1^3 \lambda_2^3} \right] [1 + \mathfrak{M} \lambda_1^2]. \quad (49)$$

A.3. Coefficients for neo-Hookean model. The components of matrices in (14) for the neo-Hookean energy density are given by

$$\begin{aligned} \mathcal{S}_{22} = & [\mathcal{U}_1 R^2 [\mathcal{U}_2^2 + \mathcal{U}_4^2] [\mathcal{S}_n^1 \mathcal{U}_2^2 + \mathcal{S}_n^2 \mathcal{U}_4^2]] \lambda_1^6 \lambda_2^2 \gamma^4 R^4, \\ \mathcal{S}_{24} = & [\mathcal{U}_1 R^2 [\mathcal{U}_2^2 + \mathcal{U}_4^2] [\mathcal{S}_n^1 \mathcal{U}_2 \mathcal{U}_4 - \mathcal{S}_n^2 \mathcal{U}_2 \mathcal{U}_4]] \lambda_1^6 \lambda_2^2 \gamma^4 R^4, \\ \mathcal{S}_{42} = & \mathcal{S}_{24}, \\ \mathcal{S}_{44} = & [\mathcal{U}_1 R^2 [\mathcal{U}_2^2 + \mathcal{U}_4^2] [\mathcal{S}_n^1 \mathcal{U}_4^2 + \mathcal{S}_n^2 \mathcal{U}_2^2]] \lambda_1^6 \lambda_2^2 \gamma^4 R^4, \end{aligned} \quad (50)$$

and

$$\begin{aligned} \mathcal{V}_1 = & [\mathcal{V}_n^2 \mathcal{U}_1 \mathcal{U}_2 [\mathcal{U}_2^2 + \mathcal{U}_4^2]^2 \gamma R \sin \theta + \mathcal{V}_n^3] [\mathcal{U}_2^2 + \mathcal{U}_4^2]^3 R^2] \lambda_1^6 \lambda_2^2 \gamma^4 R^4 \\ & - [\mathcal{V}_n^1 \mathcal{U}_2 [\mathcal{U}_2^2 + \mathcal{U}_4^2]^2] \lambda_1^6 \lambda_2^2 \gamma^4 R^4 - \frac{1}{2} P \mathcal{U}_1 \mathcal{U}_4 [\mathcal{U}_2^2 + \mathcal{U}_4^2]^{3/2} \lambda_1^{11} \lambda_2^5 \gamma^{10} R^{10}, \\ \mathcal{V}_2 = & [\mathcal{V}_n^2 \mathcal{U}_1 \mathcal{U}_4 [\mathcal{U}_2^2 + \mathcal{U}_4^2]^2 \gamma R \sin \theta] \lambda_1^6 \lambda_2^2 \gamma^4 R^4 - [\mathcal{V}_n^1 \mathcal{U}_4 [\mathcal{U}_2^2 + \mathcal{U}_4^2]^2] \lambda_1^6 \lambda_2^2 \gamma^4 R^4 \\ & + \frac{1}{2} P \mathcal{U}_1 \mathcal{U}_2 [\mathcal{U}_2^2 + \mathcal{U}_4^2]^{3/2} \lambda_1^{11} \lambda_2^5 \gamma^{10} R^{10}, \end{aligned} \quad (51)$$

along with

$$\begin{aligned} S_n^1 &= [\mathcal{U}_2^2 + \mathcal{U}_4^2]^2 \mathcal{U}_1^2 R^2 + 3\gamma^4 R^4, & S_n^2 &= [\mathcal{U}_2^2 + \mathcal{U}_4^2]^2 \mathcal{U}_1^2 R^2 - \gamma^4 R^4, \\ \mathcal{V}_n^1 &= 2[\mathcal{U}_2 R + \mathcal{U}_1 \gamma \sin \theta] \gamma^4 R^5, & \mathcal{V}_n^2 &= [\mathcal{U}_2^2 + \mathcal{U}_4^2]^2 \mathcal{U}_1^2 R^2 - \gamma^4 R^4, & \mathcal{V}_n^3 &= [\mathcal{U}_2^2 + \mathcal{U}_4^2] \mathcal{U}_1^4 \gamma^2 - \gamma^4 R^4, \\ P &= \frac{\widehat{P} R_b}{\frac{1}{2} \mu_1 T}. \end{aligned} \quad (52)$$

Nondimensional principal Cauchy stresses in the θ - and ϕ -directions are computed as

$$\sigma_{\theta\theta} = 2 \left[\frac{\lambda_1}{\lambda_2} - \frac{1}{\lambda_1^3 \lambda_2^3} \right], \quad \sigma_{\phi\phi} = 2 \left[\frac{\lambda_2}{\lambda_1} - \frac{1}{\lambda_1^3 \lambda_2^3} \right]. \quad (53)$$

A.4. Matrix coefficients for wrinkled region. In the wrinkled region, using the relaxed energy density obtained by substituting $\lambda_2 = 1/\sqrt{\lambda_1}$, we find that the terms S_{22} , S_{24} , S_{42} , S_{44} , \mathcal{V}_1 , \mathcal{V}_2 for each of the material models discussed above are modified as below.

For Ogden energy density, we get

$$\begin{aligned} S_{22} &= \mu_1^* R \left[\varrho_\theta^2 \left[[\alpha_1 - 1] \lambda_1^{3\alpha_1/2} + \left[\frac{1}{2} \alpha_1 + 1 \right] \right] + \eta_\theta^2 [\lambda_1^{3\alpha_1/2} - 1] \right] \lambda_1^{(\alpha_2 + \alpha_3)/2 + 8} \\ &\quad + \mu_2^* R \left[\varrho_\theta^2 \left[[\alpha_2 - 1] \lambda_1^{3\alpha_2/2} + \left[\frac{1}{2} \alpha_2 + 1 \right] \right] + \eta_\theta^2 [\lambda_1^{3\alpha_2/2} - 1] \right] \lambda_1^{(\alpha_1 + \alpha_3)/2 + 8} \\ &\quad + \mu_3^* R \left[\varrho_\theta^2 \left[[\alpha_3 - 1] \lambda_1^{3\alpha_3/2} + \left[\frac{1}{2} \alpha_3 + 1 \right] \right] + \eta_\theta^2 [\lambda_1^{3\alpha_3/2} - 1] \right] \lambda_1^{(\alpha_1 + \alpha_2)/2 + 8}, \\ S_{24} &= \mu_1^* R \left[\varrho_\theta \eta_\theta \left[[\alpha_1 - 2] \lambda_1^{3\alpha_1/2} + \left[\frac{1}{2} \alpha_1 + 2 \right] \right] \right] \lambda_1^{(\alpha_2 + \alpha_3)/2 + 8} \\ &\quad + \mu_2^* R \left[\varrho_\theta \eta_\theta \left[[\alpha_2 - 2] \lambda_1^{3\alpha_2/2} + \left[\frac{1}{2} \alpha_2 + 2 \right] \right] \right] \lambda_1^{(\alpha_1 + \alpha_3)/2 + 8} \\ &\quad + \mu_3^* R \left[\varrho_\theta \eta_\theta \left[[\alpha_3 - 2] \lambda_1^{3\alpha_3/2} + \left[\frac{1}{2} \alpha_3 + 2 \right] \right] \right] \lambda_1^{(\alpha_1 + \alpha_2)/2 + 8}, \\ S_{42} &= S_{24}, \\ S_{44} &= \mu_1^* R \left[\eta_\theta^2 \left[[\alpha_1 - 1] \lambda_1^{3\alpha_1/2} + \left[\frac{1}{2} \alpha_1 + 1 \right] \right] + \varrho_\theta^2 [\lambda_1^{3\alpha_1/2} - 1] \right] \lambda_1^{(\alpha_2 + \alpha_3)/2 + 8} \\ &\quad + \mu_2^* R \left[\eta_\theta^2 \left[[\alpha_2 - 1] \lambda_1^{3\alpha_2/2} + \left[\frac{1}{2} \alpha_2 + 1 \right] \right] + \varrho_\theta^2 [\lambda_1^{3\alpha_2/2} - 1] \right] \lambda_1^{(\alpha_1 + \alpha_3)/2 + 8} \\ &\quad + \mu_3^* R \left[\eta_\theta^2 \left[[\alpha_3 - 1] \lambda_1^{3\alpha_3/2} + \left[\frac{1}{2} \alpha_3 + 1 \right] \right] + \varrho_\theta^2 [\lambda_1^{3\alpha_3/2} - 1] \right] \lambda_1^{(\alpha_1 + \alpha_2)/2 + 8}, \end{aligned} \quad (54)$$

along with

$$\begin{aligned} \mathcal{V}_1 &= \left[\mu_1^* [\lambda_1^{3\alpha_1/2} - 1] \lambda_1^{(\alpha_2 + \alpha_3)/2 + 10} + \mu_2^* [\lambda_1^{3\alpha_2/2} - 1] \lambda_1^{(\alpha_1 + \alpha_3)/2 + 10} \right. \\ &\quad \left. + \mu_3^* [\lambda_1^{3\alpha_3/2} - 1] \lambda_1^{(\alpha_1 + \alpha_2)/2 + 10} \right] \gamma^3 \mathcal{U}_2 \sin \theta \\ &\quad - \frac{1}{2} \mu_1^* P \mathcal{U}_1 \mathcal{U}_4 \lambda_1^{(\alpha_1 + \alpha_2 + \alpha_3)/2 + 12} \gamma^3, \\ \mathcal{V}_2 &= \left[\mu_1^* [\lambda_1^{3\alpha_1/2} - 1] \lambda_1^{(\alpha_2 + \alpha_3)/2 + 10} + \mu_2^* [\lambda_1^{3\alpha_2/2} - 1] \lambda_1^{(\alpha_1 + \alpha_3)/2 + 10} \right. \\ &\quad \left. + \mu_3^* [\lambda_1^{3\alpha_3/2} - 1] \lambda_1^{(\alpha_1 + \alpha_2)/2 + 10} \right] \gamma^3 \mathcal{U}_4 \sin \theta \\ &\quad + \frac{1}{2} \mu_1^* P \mathcal{U}_1 \mathcal{U}_2 \lambda_1^{(\alpha_1 + \alpha_2 + \alpha_3)/2 + 12} \gamma^3, \\ P &= \frac{2 \widehat{P} R_b}{\mu_1 T}. \end{aligned} \quad (55)$$

For Mooney–Rivlin energy density, we get

$$\begin{aligned} S_{22} &= R[\varrho_\theta^2[\lambda_1^4+2\lambda_1+3\mathfrak{M}]+\eta_\theta^2[\lambda_1^4-\lambda_1+\mathfrak{M}[\lambda_1^3-1]]], \\ S_{24} &= R[\varrho_\theta\eta_\theta[3\lambda_1+4\mathfrak{M}-\mathfrak{M}\lambda_1^3]], \\ S_{42} &= S_{24}, \\ S_{44} &= R[\eta_\theta^2[\lambda_1^4+2\lambda_1+3\mathfrak{M}]+\varrho_\theta^2[\lambda_1^4-\lambda_1+\mathfrak{M}[\lambda_1^3-1]]], \end{aligned} \tag{56}$$

along with

$$\begin{aligned} \nu_1 &= [\lambda_1^4-\lambda_1+\mathfrak{M}[\lambda_1^3-1]]\gamma^3\lambda_1^2\mathcal{U}_2 \sin \theta - [[\frac{1}{2}P]\mathcal{U}_1\mathcal{U}_4\lambda_1^6\gamma^3], \\ \nu_2 &= [\lambda_1^4-\lambda_1+\mathfrak{M}[\lambda_1^3-1]]\gamma^3\lambda_1^2\mathcal{U}_4 \sin \theta + [[\frac{1}{2}P]\mathcal{U}_1\mathcal{U}_2\lambda_1^6\gamma^3]. \end{aligned} \tag{57}$$

For neo-Hookean energy density, we get

$$\begin{aligned} S_{22} &= R[\varrho_\theta^2[\lambda_1^4+2\lambda_1]+\eta_\theta^2[\lambda_1^4-\lambda_1]], & S_{24} &= R[\varrho_\theta\eta_\theta[3\lambda_1]], \\ S_{42} &= S_{24}, & S_{44} &= R[\eta_\theta^2[\lambda_1^4+2\lambda_1]+\varrho_\theta^2[\lambda_1^4-\lambda_1]], \end{aligned} \tag{58}$$

and

$$\nu_1 = [\lambda_1^4-\lambda_1]\gamma^3\lambda_1^2\mathcal{U}_2 \sin \theta - [[\frac{1}{2}P]\mathcal{U}_1\mathcal{U}_4\lambda_1^6\gamma^3], \tag{59}$$

$$\nu_2 = [\lambda_1^4-\lambda_1]\gamma^3\lambda_1^2\mathcal{U}_4 \sin \theta + [[\frac{1}{2}P]\mathcal{U}_1\mathcal{U}_2\lambda_1^6\gamma^3]. \tag{60}$$

Acknowledgements

Major portion of this work was conducted when both the authors were based at IIT Hyderabad. This work was financially supported by a research grant associated with the Ramanujan fellowship by the Science and Engineering Research Board (Sanction No: SB/S2/RJN-116/2015) awarded to Saxena.

References

[Başar and Itskov 1998] Y. Başar and M. Itskov, “Finite element formulation of the Ogden material model with application to rubber-like shells”, *Int. J. Numer. Methods Eng.* **42**:7 (1998), 1279–1305.

[Barsotti 2015] R. Barsotti, “Approximated solutions for axisymmetric wrinkled inflated membranes”, *J. Appl. Mech. (ASME)* **82**:11 (2015), art. id. 111007.

[Benedict et al. 1979] R. Benedict, A. Wineman, and W. H. Yang, “The determination of limiting pressure in simultaneous elongation and inflation of nonlinear elastic tubes”, *Int. J. Solids Struct.* **15**:3 (1979), 241–249.

[Bonadies 1987] M. Bonadies, “Asymptotic behaviour of inflated toroidal elastic membranes”, *Rend. Sem. Mat. Univ. Politec. Torino* **45**:3 (1987), 63–74.

[Budiansky 1974] B. Budiansky, “Theory of buckling and post-buckling behavior of elastic structures”, *Adv. Appl. Mech.* **14** (1974), 1–65.

[Carroll 1987] M. M. Carroll, “Pressure maximum behavior in inflation of incompressible elastic hollow spheres and cylinders”, *Quart. Appl. Math.* **45**:1 (1987), 141–154.

[Clark 1950] R. A. Clark, “On the theory of thin elastic toroidal shells”, *J. Math. Phys.* **29**:1-4 (1950), 146–178.

[Dreyer et al. 1982] W. Dreyer, I. Müller, and P. Strehlow, “A study of equilibria of interconnected balloons”, *Quart. J. Mech. Appl. Math.* **35**:3 (1982), 419–440.

[Epstein 1999] M. Epstein, “On the wrinkling of anisotropic elastic membranes”, *J. Elasticity* **55**:2 (1999), 99–109.

- [Gruttmann and Taylor 1992] F. Gruttmann and R. L. Taylor, “Theory and finite element formulation of rubberlike membrane shells using principal stretches”, *Int. J. Numer. Methods Eng.* **35**:5 (1992), 1111–1126.
- [Harold 1970] M. E. Harold, “Load transfer via a wrinkled membrane”, *Proc. R. Soc. Lond. A* **316**:1525 (1970), 269–289.
- [Haughton and McKay 1995] D. M. Haughton and B. A. McKay, “Wrinkling of annular discs subjected to radial displacements”, *Int. J. Eng. Sci.* **33**:3 (1995), 335–350.
- [Hill 1980] J. M. Hill, “The finite inflation of a thick-walled elastic torus”, *Quart. J. Mech. Appl. Math.* **33**:4 (1980), 471–490.
- [Holzapfel 2000] G. A. Holzapfel, *Nonlinear solid mechanics: a continuum approach for engineering*, Wiley, Chichester, UK, 2000.
- [Holzapfel et al. 1996] G. A. Holzapfel, R. Eberlein, P. Wriggers, and H. W. Weizsäcker, “A new axisymmetrical membrane element for anisotropic, finite strain analysis of arteries”, *Commun. Numer. Methods Eng.* **12**:8 (1996), 507–517.
- [Horný et al. 2006] L. Horný, R. Žitný, H. Chlup, and H. Macková, “Identification of the material parameters of an aortic wall”, *Bull. Appl. Mech.* **2**:8 (2006), 173–181.
- [Humphrey 1998] J. D. Humphrey, “Computer methods in membrane biomechanics”, *Comput. Methods Biomech. Biomed. Engin.* **1**:3 (1998), 171–210.
- [Jenkins et al. 1998] C. H. Jenkins, F. Haugen, and W. H. Spicher, “Experimental measurement of wrinkling in membranes undergoing planar deformation”, *Exp. Mech.* **38**:2 (1998), 147–152.
- [Jordan 1962] P. F. Jordan, “Stresses and deformations of the thin-walled pressurized torus”, *J. Aerosp. Sci.* **29**:2 (1962), 213–225.
- [Kanner and Horgan 2007] L. M. Kanner and C. O. Horgan, “Elastic instabilities for strain-stiffening rubber-like spherical and cylindrical thin shells under inflation”, *Int. J. Non-Linear Mech.* **42**:2 (2007), 204–215.
- [Khayat et al. 1992] R. E. Khayat, A. Derdorri, and A. Garcia-Réjon, “Inflation of an elastic cylindrical membrane: non-linear deformation and instability”, *Int. J. Solids Struct.* **29**:1 (1992), 69–87.
- [Koiter 1945] W. T. Koiter, *The stability of elastic equilibrium*, Ph.D. thesis, Technische Hooge School, 1945, Available at <https://tinyurl.com/koiterphd>.
- [Kydoniefs and Spencer 1965] A. D. Kydoniefs and A. J. M. Spencer, “The finite inflation of an elastic torus”, *Int. J. Eng. Sci.* **3**:2 (1965), 173–195.
- [Kydoniefs and Spencer 1967] A. D. Kydoniefs and A. J. M. Spencer, “The finite inflation of an elastic toroidal membrane of circular cross section”, *Int. J. Eng. Sci.* **5**:4 (1967), 367–391.
- [Li and Steigmann 1995a] X. Li and D. J. Steigmann, “Finite deformation of a pressurized toroidal membrane”, *Int. J. Non-Linear Mech.* **30**:4 (1995), 583–595.
- [Li and Steigmann 1995b] X. Li and D. J. Steigmann, “Point loads on a hemispherical elastic membrane”, *Int. J. Non-Linear Mech.* **30**:4 (1995), 569–581.
- [Liepins and Sanders 1963] A. Liepins and J. L. Sanders, “Toroidal membrane under internal pressure”, *AIAA J.* **1**:9 (1963), 2105–2110.
- [Mansfield 1981] E. H. Mansfield, “Gravity-induced wrinkle lines in vertical membranes”, *Proc. R. Soc. Lond. A* **375**:1762 (1981), 307–325.
- [Müller and Struchtrup 2002] I. Müller and H. Struchtrup, “Inflating a rubber balloon”, *Math. Mech. Solids* **7**:5 (2002), 569–577.
- [Nayyar et al. 2011] V. Nayyar, K. Ravi-Chandar, and R. Huang, “Stretch-induced stress patterns and wrinkles in hyperelastic thin sheets”, *Int. J. Solids Struct.* **48**:25-26 (2011), 3471–3483.
- [Ogden 1972] R. W. Ogden, “Large deformation isotropic elasticity: on the correlation of theory and experiment for incompressible rubberlike solids”, *Proc. R. Soc. Lond. A* **326**:1567 (1972), 565–584.
- [Papargyri 1995] S. Papargyri-Pegiou, “Stability of the axisymmetric analytical and numerical solutions in a thin-walled pressurized torus of compressible nonlinear elastic material”, *Int. J. Eng. Sci.* **33**:7 (1995), 1005–1025.
- [Papargyri 2005] S. Papargyri-Beskou, “Finite-element analysis of an axisymmetric, thin-walled, nonlinear elastic pressurized torus”, *Acta Mech.* **178**:1-2 (2005), 1–22.

- [Papargyri and Stavrakakis 2000] S. Papargyri-Pegiou and E. Stavrakakis, “Axisymmetric numerical solutions of a thin-walled pressurized torus of incompressible nonlinear elastic materials”, *Comput. Struct.* **77**:6 (2000), 747–757.
- [Patil et al. 2015] A. Patil, A. Nordmark, and A. Eriksson, “Wrinkling of cylindrical membranes with non-uniform thickness”, *Eur. J. Mech. A Solids* **54** (2015), 1–10.
- [Pipkin 1986] A. C. Pipkin, “The relaxed energy density for isotropic elastic membranes”, *IMA J. Appl. Math.* **36**:1 (1986), 85–99.
- [Reddy and Saxena 2017] N. H. Reddy and P. Saxena, “Limit points in the free inflation of a magnetoelastic toroidal membrane”, *Int. J. Non-Linear Mech.* **95** (2017), 248–263.
- [Reddy and Saxena 2018] N. H. Reddy and P. Saxena, “Instabilities in the axisymmetric magnetoelastic deformation of a cylindrical membrane”, *Int. J. Solids Struct.* **136-137** (2018), 203–219.
- [Roxburgh 1995] D. G. Roxburgh, “Inflation of nonlinearly deformed annular elastic membranes”, *Int. J. Solids Struct.* **32**:14 (1995), 2041–2052.
- [Roychowdhury and DasGupta 2015] S. Roychowdhury and A. DasGupta, “Inflating a flat toroidal membrane”, *Int. J. Solids Struct.* **67-68** (2015), 182–191.
- [Saxena et al. 2019] P. Saxena, N. H. Reddy, and S. P. Pradhan, “Magnetoelastic deformation of a circular membrane: wrinkling and limit point instabilities”, *Int. J. Non-Linear Mech.* **116** (2019), 250–261.
- [Shang and Cheng 1991] X.-c. Shang and C.-j. Cheng, “Instability of toroidal membrane with large tensile deformation”, *Appl. Math. Mech.* **12**:6 (1991), 557–564.
- [Steigmann 1990] D. J. Steigmann, “Tension-field theory”, *Proc. R. Soc. Lond. A* **429**:1876 (1990), 141–173.
- [Steigmann 2005] D. J. Steigmann, “Puncturing a thin elastic sheet”, *Int. J. Non-Linear Mech.* **40**:2-3 (2005), 255–270.
- [Stein and Hedgepeth 1961] M. Stein and J. M. Hedgepeth, “Analysis of partly wrinkled membranes”, technical note D-813, NASA, 1961.
- [Szyszkowski and Glockner 1987] W. Szyszkowski and P. G. Glockner, “Spherical membranes subjected to vertical concentrated loads: an experimental study”, *Eng. Struct.* **9**:3 (1987), 183–192.
- [Tamadapu and DasGupta 2012] G. Tamadapu and A. DasGupta, “In-plane surface modes of an elastic toroidal membrane”, *Int. J. Eng. Sci.* **60** (2012), 25–36.
- [Tamadapu and DasGupta 2014] G. Tamadapu and A. DasGupta, “Effect of curvature and anisotropy on the finite inflation of a hyperelastic toroidal membrane”, *Eur. J. Mech. A Solids* **46** (2014), 106–114.
- [Tamadapu et al. 2013] G. Tamadapu, N. N. Dhavale, and A. DasGupta, “Geometrical feature of the scaling behavior of the limit-point pressure of inflated hyperelastic membranes”, *Phys. Rev. E* **88**:5 (2013), art. id. 053201.
- [Wang et al. 2017] F. Wang, C. Yuan, T. Lu, and T. J. Wang, “Anomalous bulging behaviors of a dielectric elastomer balloon under internal pressure and electric actuation”, *J. Mech. Phys. Solids* **102** (2017), 1–16.
- [Wong and Pellegrino 2006] Y. W. Wong and S. Pellegrino, “Wrinkled membranes, II: Analytical models”, *J. Mech. Mater. Struct.* **1**:1 (2006), 27–61.
- [Wriggers and Taylor 1990] P. Wriggers and R. L. Taylor, “A fully non-linear axisymmetrical membrane element for rubber-like materials”, *Eng. Computation.* **7**:4 (1990), 303–310.
- [Wu 1974] C. H. Wu, “The wrinkled axisymmetric air bags made of inextensible membrane”, *J. Appl. Math. (ASME)* **41**:4 (1974), 963–968.
- [Wu 1978] C.-H. Wu, “Nonlinear wrinkling of nonlinear membranes of revolution”, *J. Appl. Mech. (ASME)* **45**:3 (1978), 533–538.
- [Wu and Canfield 1981] C. H. Wu and T. R. Canfield, “Wrinkling in finite plane-stress theory”, *Quart. Appl. Math.* **39**:2 (1981), 179–199.
- [Yang and Feng 1970] W. H. Yang and W. W. Feng, “On axisymmetrical deformations of nonlinear membranes”, *J. Appl. Mech. (ASME)* **37**:4 (1970), 1002–1011.
- [Zak 1982] M. Zak, “Statics of wrinkling films”, *J. Elasticity* **12**:1 (1982), 51–63.

Received 7 Jan 2019. Revised 1 Aug 2019. Accepted 7 Aug 2019.

SAIRAM PAMULAPARTHI VENKATA: sairampv44@gmail.com

Department of Mechanical and Aerospace Engineering, Field of Theoretical and Applied Mechanics, Cornell University, Ithaca, NY, United States

and

Department of Mechanical and Aerospace Engineering, Indian Institute of Technology Hyderabad, Telangana, India

PRASHANT SAXENA: prashant.saxena@glasgow.ac.uk

Glasgow Centre for Computational Engineering, James Watt School of Engineering, University of Glasgow, Glasgow, United Kingdom

and

Department of Mechanical and Aerospace Engineering, Indian Institute of Technology Hyderabad, Telangana, India

JOURNAL OF MECHANICS OF MATERIALS AND STRUCTURES

msp.org/jomms

Founded by Charles R. Steele and Marie-Louise Steele

EDITORIAL BOARD

| | |
|-----------------------|--|
| ADAIR R. AGUIAR | University of São Paulo at São Carlos, Brazil |
| KATIA BERTOLDI | Harvard University, USA |
| DAVIDE BIGONI | University of Trento, Italy |
| MAENGHYO CHO | Seoul National University, Korea |
| HUILING DUAN | Beijing University |
| YIBIN FU | Keele University, UK |
| IWONA JASIUK | University of Illinois at Urbana-Champaign, USA |
| DENNIS KOCHMANN | ETH Zurich |
| MITSUTOSHI KURODA | Yamagata University, Japan |
| CHEE W. LIM | City University of Hong Kong |
| ZISHUN LIU | Xi'an Jiaotong University, China |
| THOMAS J. PENCE | Michigan State University, USA |
| GIANNI ROYER-CARFAGNI | Università degli studi di Parma, Italy |
| DAVID STEIGMANN | University of California at Berkeley, USA |
| PAUL STEINMANN | Friedrich-Alexander-Universität Erlangen-Nürnberg, Germany |
| KENJIRO TERADA | Tohoku University, Japan |

ADVISORY BOARD

| | |
|---------------|---|
| J. P. CARTER | University of Sydney, Australia |
| D. H. HODGES | Georgia Institute of Technology, USA |
| J. HUTCHINSON | Harvard University, USA |
| D. PAMPLONA | Universidade Católica do Rio de Janeiro, Brazil |
| M. B. RUBIN | Technion, Haifa, Israel |

PRODUCTION production@msp.org

SILVIO LEVY Scientific Editor


Cover photo: Mando Gomez, www.mandolux.com

See msp.org/jomms for submission guidelines.

JoMMS (ISSN 1559-3959) at Mathematical Sciences Publishers, 798 Evans Hall #6840, c/o University of California, Berkeley, CA 94720-3840, is published in 10 issues a year. The subscription price for 2019 is US \$635/year for the electronic version, and \$795/year (+\$60, if shipping outside the US) for print and electronic. Subscriptions, requests for back issues, and changes of address should be sent to MSP.

JoMMS peer-review and production is managed by EditFLOW® from Mathematical Sciences Publishers.

PUBLISHED BY

 **mathematical sciences publishers**
nonprofit scientific publishing

<http://msp.org/>

© 2019 Mathematical Sciences Publishers

- Extended higher-order sandwich panel theory for plates with arbitrary aspect ratios** FAISAL SIDDIQUI and GEORGE A. KARDOMATEAS 449
- Applications of extended higher order sandwich panel theory for plates with arbitrary aspect ratios** FAISAL SIDDIQUI and GEORGE A. KARDOMATEAS 461
- Instabilities in the free inflation of a nonlinear hyperelastic toroidal membrane** SAIRAM PAMULAPARTHI VENKATA and PRASHANT SAXENA 473
- Plane strain polar elasticity of fibre-reinforced functionally graded materials and structures** KONSTANTINOS P. SOLDATOS, METIN AYDOGDU and UFUK GUL 497
- Integrated modelling of tool wear and microstructural evolution internal relations in friction stir welding with worn pin profiles** ZHAO ZHANG and ZHIJUN TAN 537
- Local gradient theory for thermoelastic dielectrics: accounting for mass and electric charge transfer due to microstructure changes** OLHA HRYTSYNA and VASYL KONDRAT 549
- The effect of boundary conditions on the lowest vibration modes of strongly inhomogeneous beams** ONUR ŞAHİN 569
- Thermal stress around an arbitrary shaped nanohole with surface elasticity in a thermoelectric material** KUN SONG, HAO-PENG SONG, PETER SCHIAVONE and CUN-FA GAO 587